FINAL REPORT

Interactions between Organic Aerosol and NOy: Influence on Oxidant Production

AQRP Project 12-012

Prepared by:

Lea Hildebrandt Ruiz, The University of Texas at Austin

Greg Yarwood, ENVIRON

The University of Texas at Austin
Center for Energy and Environmental Resources
10100 Burnet Road
Bldg. 133, CEER
Austin, Texas 78758

ENVIRON International
773 San Marin Drive, Suite 2115
Novato California, 94998

Acknowledgement

Table of Contents

Figures

Tables

Executive Summary

In rural areas where emission rates of NO_x (NO + NO_2) are relatively low, ozone formation can be sensitive to secondary NO_x sources such as decomposition of organic nitrates (ONs). AQRP project 10-042 provided experimental evidence for NO_x production when ONs degrade by OH reaction and photolysis. Implementing NO_x production from OH reaction with ONs causes regional ozone increases that are large enough to affect model agreement with ozone observations. This implies that ONs are less available to NO_x recycling than previous experiments suggested. This project investigated the hypothesis that uptake of ONs into organic aerosol (OA) reduces the amount of NO_x recycled by ON photolysis and reaction with OH.

The University of Texas at Austin (UT-Austin) conducted laboratory chamber experiments to investigate the formation of organic nitrates (ON) and their gas-particle partitioning from different VOC precursors. Significant concentrations of ON formed from all precursors investigated, and NO_x concentrations decreased during each experiment providing experimental evidence that VOCs act as NO_x sinks and ON sources. A substantial fraction of the ON partitioned to the particle phase, and the gas-particle partitioning of the ON was found to be reversible. UT-Austin also measured ONs in the gas- and particle phase in ambient measurements during DISCOVER-AQ near Houston. Approximately 100 organic nitrogen species were identified in the gas-phase, and they exhibited different diurnal variation. The particle-phase ONs measured near Houston exhibited a strong diurnal cycle with lowest concentrations in the afternoon.

ENVIRON modified the Carbon Bond 6 (CB6) chemical mechanism to differentiate ONs between simple alkyl nitrates (AN) that remain in the gas-phase and multi-functional ONs that can partition into OA. Uptake of multi-functional ONs by organic aerosol (OA) was added to the Comprehensive Air quality Model with extensions (CAMx). ONs present in aerosols are then assumed to undergo hydrolysis to nitric acid with a lifetime of approximately 6 hours based on laboratory experiments and ambient data. The revised CB6 mechanism is called CB6r2 and regional modeling simulations using CAMx with CB6r2 showed improved performance in simulating ozone and in simulating the partitioning of NO_y between ONs and nitric acid.

Uncertainty in the atmospheric fate of ONs adds substantial uncertainty in modeling regional O_3 and other oxidants. Additional laboratory studies and ambient measurements are needed to better quantify partitioning of ONs to aerosol, forming ANs, and the subsequent chemical fate of ANs. We make the following recommendations for additional environmental chamber experiments and other activities to support improvements in the representation of organic nitrates in chemical transport models:

1. Environmental chamber experiments forming ONs from different precursors and at different relative humidity to quantify the hydrolysis rate of ONs. (The lifetime of 6 hours currently used in CB6r2 is based on limited experimental and ambient data.)

2. Analysis of experimental data to calculate the gas-particle partitioning coefficient of ONs (the gas-particle partitioning currently used in CB6r2 is based on a single peer-reviewed publication). This analysis necessitates quantification of ONs in the gas-phase and the particle-phase, or quantification of total ON formation and the amount of ONs in the gas-phase or particle-phase. A more systematic analysis of the gas-particle partitioning of ONs with varying environmental chamber temperature would support this analysis.

3. Analysis of ambient data to calculate the gas-particle partitioning factor of organic nitrates. This analysis would necessitate quantification of ONs in the gas-phase and the particle phase.

The ON scheme implemented in CB6r2 is simple and generally consistent with available studies and improves the performance of CB6r2 in simulating regional O_3 and NO_y speciation compared to CB6r1. CB6r2 is recommended over preceding versions of CB6 and CB05.

1.0 Introduction

The TCEQ is responsible for managing the impacts of Texas' emissions on its air quality. The Texas State Implementation Plan (SIP) includes strategies for attaining standards for ozone, particulate matter ($PM_{2.5}$) and regional haze. Regional photochemical models and their chemical mechanisms are important SIP tools because they establish quantitative linkages between primary emissions and secondary pollutants. Laboratory chamber experiments are often used to develop and test chemical mechanisms or parameterizations for the models. Ambient observations are another important tool because they allow observation of processes occurring in the complex atmosphere and testing of the regional models.

In rural areas, where NO_x emission rates are relatively low, ozone formation can be sensitive to secondary NO_x sources such as decomposition of organic nitrates ($R-ONO_2$). AQRP project 10-042 (Yarwood et al., 2012) provided experimental evidence for NO_x production when organic nitrates degrade by OH reaction and photolysis. Implementing NO_x production from OH reaction with organic nitrates causes regional ozone increases (Figure 1-1) that are large enough to affect model agreement with ozone observations. Similarly, when NO_x production from organic nitrate photolysis was implemented in CB05, NOAA found that resulting regional ozone increased and degraded the performance of the national ozone forecast model (Saylor and Stein, 2012). In short, while there is scientific evidence for occurrence of NO_x recycling from organic nitrates, implementing these reactions in current chemical mechanisms and models can degrade performance for ozone.
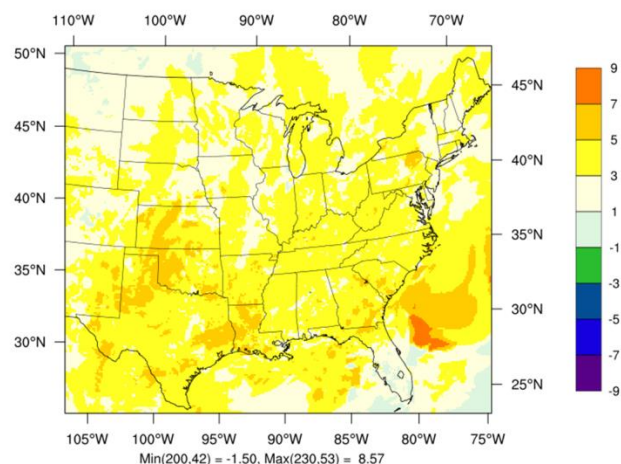
Figure 1-1. Increase in daily maximum 8-hr average O_3 (DMA8 O_3; ppb) during August 2005 when OH reaction with organic nitrates forms NO_2 rather than HNO3. DMA8 O_3 increases more than 3 ppb across most of Texas and by more than 5 ppb near Houston.

There are several potential explanations for why implementing NO_x recycling from organic nitrates can degrade model performance for ozone such as off-setting errors between model chemistry and another process (e.g. emissions), or over-estimated organic nitrate concentrations that overstate the effects of adding these reactions. Horowitz et al. (2007) systematically investigated the sensitivity of the MOZART model to organic nitrate chemistry and deposition using ICARTT data (for NO_x, NO_y and O_3) to evaluate the model. They obtained best performance by adopting low-end yields of organic nitrates from isoprene and rapid dry deposition of organic nitrates (equal to nitric acid). If organic nitrates are removed rapidly by dry deposition, organic nitrate uptake by organic aerosols also should be considered but is not included in current models (CAMx, CMAQ). Flow tube experiments presented by Perraud et al. (2012) suggest that organic aerosol growth can irreversibly incorporate organic nitrates in the aerosol phase where they are protected from decomposition to NO_x.

We proposed to investigate the hypothesis that uptake of organic nitrates into secondary organic aerosol (SOA) reduces the amount of NO_x recycled by organic nitrate photolysis and OH reaction. ENVIRON modified the CAMx model and conducted sensitivity tests to evaluate the potential importance of this process. The University of Texas at Austin (UT-Austin) conducted laboratory chamber experiments to investigate the formation of organic nitrates (ON) and their gas-particle partitioning. UT-Austin also measured ON in the gas- and particle phase in ambient measurements during DISCOVER-AQ near Houston.

2.0 Photochemical Modeling

2.1 Background

The atmospheric chemistry of ONs is reviewed by Roberts (1990), Shepson (2007), and most recently by Perring et al. (2013). The major ON formation pathway is reaction between an organic peroxy radical (RO_2) and NO in which ONs ($RONO_2$) are a minor product channel:

$$RO_2 + NO \rightarrow \alpha\ RONO_2 + (1-\alpha)\ \{RO + NO_2\} \tag{1}$$

The ON yield (α) depends upon the size and structure of the organic backbone (R) of the peroxy radical and ranges from essentially zero for R=methyl to more than 35% for large alkyl chains such as R=n-decyl. The structure of R is important and structure-activity relationships (SARs) have been developed and are used to estimate ON yields in the master chemical mechanisms (MCM; http://mcm.leeds.ac.uk/MCM/roots.htt).

RO_2 radicals are formed ubiquitously in the atmospheric degradation of VOCs initiated by reactions with OH, O_3, NO_3 or photolysis. In daylight OH-initiated reactions are dominant for all VOCs and photolysis is important for carbonyl compounds whereas at night reactions of NO_3

and O_3 with alkene bonds are important. ONs resulting from OH-initiated reactions may be alkyl nitrates (i.e., R contains only C and H) or multi-functional nitrates where R contains a substituent group such as hydroxy (OH), hydroperoxy (OOH) or a carbonyl (C=O or CHO). For example, ONs resulting from OH + alkene reactions are hydroxynitrates, ONs resulting from OH reaction with large alkanes (> C6) include hydroxynitrates, and ONs from OH reaction with aromatics have carbonyl groups. At night, RO_2 radicals formed by NO_3 addition to an alkene bond contain an NO_3 group within R and so and reaction (1) could form a di-nitrate.

ONs may undergo atmospheric reactions, most likely OH reacting with the organic backbone (R) or photolysis of the $-ONO_2$ chromophore. ON photolysis has been shown to liberate NO_2 from small ONs (Yarwood et al., 2012) and this mechanism is expected to apply for most ONs:

$$RONO_2 + hv \rightarrow NO_2 + RO \qquad\qquad\qquad (2)$$

Reactions (1) and (2) operate to sequester and then release NO_x and therefore may be termed NO_x-recycling. A representative atmospheric lifetime for ON photolysis is about 1 week meaning that NO_x-recycling via ON photolysis can operate at continental scales. For all carbon backbones (R) that are larger or more complex than a small alkyl groups (greater than ~C4) processes other than photolysis are likely to dominate ON fate, such as deposition, uptake by aerosol or reaction with OH.

The OH initiated degradation of ONs may be represented as:

$$RONO_2 + OH \rightarrow \beta R'ONO_2 + (1-\beta) \{R''=O + NO_2\} \qquad\qquad (3)$$
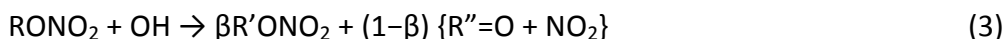
Wherein the alternate product channels either retain the nitrate group (yield = β) or release NO_2 (yield = $1-\beta$). Since OH reaction occurs on the organic backbone, retention of the nitrate group is accompanied by modification of the organic backbone and the ON produced in reaction (3) is likely to have more functional groups than the reacting ON. Elimination of NO_2 is accompanied by formation of an organic molecule that is likely to be a carbonyl (R''=O).

Little information is available on how β depends upon ON size and structure. For small alkyl (propyl and butyl) ONs β appears to be close to unity (Aschmann et al., 2011; Yarwood et al., 2012) whereas for several C6 alkyl nitrates the value of β depends upon whether the alkyl chain is straight or branched (Aschmann et al., 2011). Available results suggest greater nitrate group retention (larger β) when the site of OH reaction is distant from the nitrate group.

The presence of a nitrate group inhibits OH from abstracting nearby H-atoms thereby favoring OH reaction distant to the nitrate group and consequently favoring the nitrate retaining pathway in reaction (3). ON formation yields (α) are greater for larger and un-branched alkanes and the ONs formed from these precursors are also likely to retain their nitrate group (high β)

through subsequent product generations. Thus, nitrate retention is expected to be an important, perhaps dominant, pathway for reaction (3) in the atmosphere.

ONs from isoprene (INs) play an important role in the atmosphere because isoprene dominates VOC emission in many locations. The initial yield of ONs (α) from OH reaction is about 10% (Paulot et al., 2009) but the resulting ONs degrade rapidly because they contain an alkene bond. Analyses of ambient data suggest substantial nitrate group retention for INs in aggregate (Horowitz et al., 2007; Perring et al., 2009). Perring et al. deduced paired values of α and β for isoprene nitrates that are consistent with ambient data and for α = 10% (Paulot et al., 2009) Perring et al. recommend $\beta \approx 80\%$. The aggregate nitrate retention for INs derived by Perring et al. ($\beta \approx 80\%$) is greater than derived by than Horowitz et al. ($\beta \approx 50\%$) or Paulot et al. ($\beta \approx 30\%$) indicating uncertainty in the chemical fate of INs. The β for INs in CB6r1 based on Paulot et al. is at the low end of these estimates and should be reconsidered in the future.

The number and type of substituent groups contained by multi-functional ONs will influence their physical properties such as vapor pressure, water solubility and Henry constant, as reviewed by Perring et al. (2013). Alkyl nitrates have low water solubility and therefore small Henry constants and are removed slowly from the atmosphere by deposition (Kames and Schurath, 1992). Hydroxy nitrates resulting from alkenes and larger alkanes have Henry constants comparable to nitric acid therefore and may be deposited rapidly (Shepson et al., 1996).

ONs are formed in "high NO$_x$" environments but because their atmospheric lifetimes are hours to days they are likely to undergo subsequent chemical reactions in "low NO$_x$" environments where RO$_2$ radicals react primarily with peroxy radicals (mainly HO$_2$) rather than NO. Consequently, ON degradation products that retain the nitrate group are likely to gain a hydroperoxy group ($-$OOH) when they react. ONs formed by NO$_3$ reaction with alkenes also are likely to contain a hydroperoxy group because NO$_3$ and NO do not occur together. The presence of hydroperoxy groups is known to lower the vapor pressure of organic compounds and favor partitioning to the aerosol phase. Numerous studies have identified ONs in ambient organic aerosol (as reviewed by Perring et al., 2013) and others have shown that larger, multi-functional ONs partition almost exclusively to the aerosol phase (Matsunaga et al., 2009). Thus, ONs from large precursors (e.g., aromatics, terpenes, large alkanes) and chemically aged ONs from smaller precursors (anthropogenic alkenes, isoprene and smaller alkanes) should be expected to partition into aerosols.

The behavior of ONs in aerosol is uncertain but understanding the fate of so-called aerosol nitrates (ANs) is important for determining availability of ONs to participate in the gas-phase reactions (1 and 2) that lead to NO$_x$ recycling. The conventional model for organic aerosol (OA) formation assumes that OA constituents exist in equilibrium between the vapor and condensed

phases with partitioning determined by their vapor pressure and the volume of OA available to form an organic solution (Pankow, 1994). Perraud et al. (2012) reported non-equilibrium partitioning of ONs with nitrate molecules becoming permanently embedded in aerosol particles; however, experiments performed in this study found that ONs were able to migrate reversibly between the vapor and condensed phases.

Liu et al. (2012) exposed ANs to humidity and observed that their hydrolysis formed nitric acid within aerosol particles. The hydrolysis rate was somewhat sensitive to the relative humidity with the rate reduced for RH below about 40% but above this threshold the hydrolysis lifetime was about 6 hours. A literature review by Liu et al. of liquid phase chemistry for ONs supports the occurrence of AN hydrolysis and indicates that the structure of the nitrate group may determine the hydrolysis rate with tertiary nitrate groups being most reactive. Ambient data also indicate that ONs are lost from aerosols (Day et al., 2010). Thus, hydrolysis of ONs in aerosol is expected to occur in the atmosphere and may be the dominant removal mechanism for many ONs.

2.2 Mechanism Updates in CB6r2

The current version of CB6 is revision 1 (CB6r1) was developed in AQRP project 10-042 (Yarwood et al., 2012) and the version developed here is called CB6r2. CB6r1 includes the following types of ON:

- INTR represents ONs from isoprene that contain an alkene bond and therefore react rapidly with OH
- CRON represents nitrocresols formed from aromatic hydrocarbons that photolyze to form HONO
- NTR represents all other types of ONs formed from alkanes, alkenes, aromatics and oxygenated VOCs

The reactions of INTR and CRON are unchanged from CB6r1 in CB6r2 because they react rapidly with OH and hydrolysis in aerosols is unlikely to be competitive.

The reactions of NTR in CB6r2 are revised from CB6r1 to permit a basic representation of differing tendencies for ONs to partition into OA with consequent influence on their dominant degradation pathway. The ONs that are represented by NTR in CB6r1 are represented by NTR1 or NTR2 in CB6r2, where:

- NTR1 represents ONs that exist almost exclusively in the gas phase, mainly alky nitrates and hydroxyalkyl nitrates
- NTR2 represents ONs that can partition significantly to OA such as larger multi-functional ONs formed from aromatics and terpenes and from NTR1

NTR1 degrades by reaction with OH and photolysis. Photolysis of NTR1 liberates NO_2 and therefore represents a pathway to NOx recycling. Reaction of NTR1 with OH is assumed to add a functional group to the ON molecule rather than liberate NO_2 and consequently OH reaction converts NTR1 to NTR2 in CB6r2.

NTR2 is assumed to undergo reaction with OH or hydrolysis within aerosols. The N-containing product of the OH reaction of NTR2 would also be represented as NTR2 making explicit inclusion of the OH + NTR2 reaction unnecessary. Photolysis of NTR2 is assumed to be too slow to compete with hydrolysis.

These are the reactions of NTR1 and NTR2 in CB6r2:

$$NTR1 + hv \rightarrow NO_2 \tag{4}$$

$$NTR1 + OH \rightarrow NTR2 \tag{5}$$

$$NTR2 + H_2O_{(aer)} \rightarrow HNO_3 \tag{6}$$

The CB6r2 reaction scheme for NTR1 and NTR2 keeps track of N but does not track other products such as radicals and organic fragments because the atmospheric lifetime of NTR1 is about 1 week for photolysis and 1 day for OH-reaction, making NTR1 destruction likely to occur in low-NO_x environments where NO_x is scarce and radicals are abundant. The rate constant for OH reaction with NTR1 is 2×10^{-12} cm^3 $molecule^{-1}$ s^{-1} which is consistent with a 6-carbon alkyl nitrate (MCM; http://mcm.leeds.ac.uk/MCM/roots.htt).

The rate of NTR2 hydrolysis in aerosols and depends both upon the partitioning coefficient to aerosol and the hydrolysis rate in aerosol. In CAMx, reaction 6 is implemented as a gas-phase reaction with a pseudo gas-phase rate constant computed to give the correct rate of NTR2 hydrolysis.

The pseudo gas-phase rate of hydrolysis for NTR2 (reaction 6) is calculated as follows. Let F_P be the particle fraction of NTR2 and the initial concentration of total NTR2 be C_0. Then:

Initial concentration of NTR2 in the particle phase = $F_P C_0$

Initial concentration of NTR2 in the vapor phase = $(1-F_P) C_0$

With 1st-order hydrolysis rate constant k, the concentration of total NTR2 at time t is:

$$C(t) = (1-F_P) C_0 + F_P C_0 \exp(-kt)$$
$$\cong C_0 \exp(-F_P kt)$$

Therefore, the particle-phase hydrolysis (reaction 6) can be simulated by the following gas-phase reaction with pseudo first-order rate constant (k') a function of relative humidity (RH) as described by Liu et al. (2012):

NTR2 → HNO$_3$ (7)

$k' = F_P k$ when RH ≥ 40%

$k' = F_P k$ (RH − 20%)/(40% − 20%)   when 20% ≤ RH < 40%

$k' = 0$ when RH < 20%

Rollins et al. (2013) characterized the particle fraction of total ON (F_{P0}) in Bakersfield, CA during the 2010 CalNex campaign using a 2-product model (Odum et al., 1996):

$F_{P0} = 0.34 / (1 + 0.73/C_{OA}) + 0.66 / (1 + 1000/C_{OA})$

Where C_{OA} is the total OA concentration ($\mu g/m^3$) measured in ambient air or provided by CAMx.

To derive the partitioning coefficient for NTR2 (F_P) from that for total ON (F_{P0}) we classified the ONs measured in Bakersfield (Rollins et al., 2013) as either NTR1 or NTR2 and found that on average NTR2 comprised 71% of the observed total ON. Therefore:

$F_P = F_{P0} / 0.71$ (8)

The pseudo gas-phase hydrolysis NTR2 is modeled using equation (7) with rate constant k' computed using F_P from equation (7) and k = 4 day^{-1} (Liu et al., 2012).

A complete listing of the reactions in CB6r2 is given in Appendix A.

2.3 Box Modeling

A box model was used in developing the gas-phase chemistry for ONs in CB6r2. Simulations lasted for 48 hours with emissions occurring only during the first 24 hours in order to create a period of ON formation followed by a period of ON destruction. Separate cases were modeled with urban and rural VOC composition as summarized in Table 2-1. The total NO$_x$ in the urban and rural VOC cases was adjusted (by varying the initial NO$_x$) to produce O$_3$ peaks of about 125 ppb on the first day. Time-series comparisons for O$_3$, OH, NO$_2$ and NTR are shown in Figure 2-1 (for CB6r2 NTR shows the sum of NTR1 and NTR2.) Aerosol chemistry was not included in the box model and there was no hydrolysis of NTR2 to HNO$_3$ for CB6r2, simplifications that are useful because they enable direct comparison of ON concentrations as shown in Figure 2-1.

Table 2-1. Conditions for box model simulations.

Chemical Mechanisms	CB05, CB6r1 and CB6r2
Duration	48 hours
Ambient Conditions	1 atmosphere pressure at 298 K with 15,000 ppm water vapor
Sunlight	Clear skies at 34°N in June
Initial O_3	40 ppb
Initial CO	150 ppb
Initial VOC	Urban: AVOC = 40 ppbC, BVOC = 10 ppbC Rural: AVOC = 20 ppbC, BVOC = 8 ppbC
Initial NO_x	Urban: 10 ppb Rural: 4 ppb
Day 1 Emissions	Urban: NO_x = 17.5 ppb, AVOC = 100 ppbC, BVOC = 100 ppbC, CO = 100 ppb Rural: NO_x = 17.5 ppb, AVOC = 10 ppbC, BVOC = 190 ppbC, CO = 10 ppb
Day 2 Emissions	None
VOC/NO_x	Urban: 9.1 ppbC/ppb Rural: 10.1 ppbC/ppb

In the box model (Figure 2-1) O_3 production occurs primarily on the first day during the period when ozone precursors are emitted. The first night is a period of O_3 destruction (primarily via reactions of NO_3) and then O_3 production resumes on the second day but is slower than on the first day because less NO_2 is available. On the second day NO_x recycling from ONs can influence the availability of NO_2 as seen most clearly by comparing NTR and NO_2 for CB6r1 and CB6r2: CB6r1 has net destruction of NTR on the second day and consequently has more NO_2 and more O_3 production than CB6r2. These comments apply equally to the cases with urban and rural VOC composition.

Comparing the CB6 mechanisms to CB05 in Figure 2-1, both CB6r1 and CB6r2 produce more O_3 than CB05 on the first day which is consistent with the CB6 mechanisms producing much higher OH. Higher OH with the CB6 mechanisms is more pronounced for the rural VOC case and on the second day which is consistent with updates to isoprene chemistry introduced in CB6r1 (and unaltered in CB6r2) that boost OH production, especially at low NO_x (Yarwood et al., 2012).
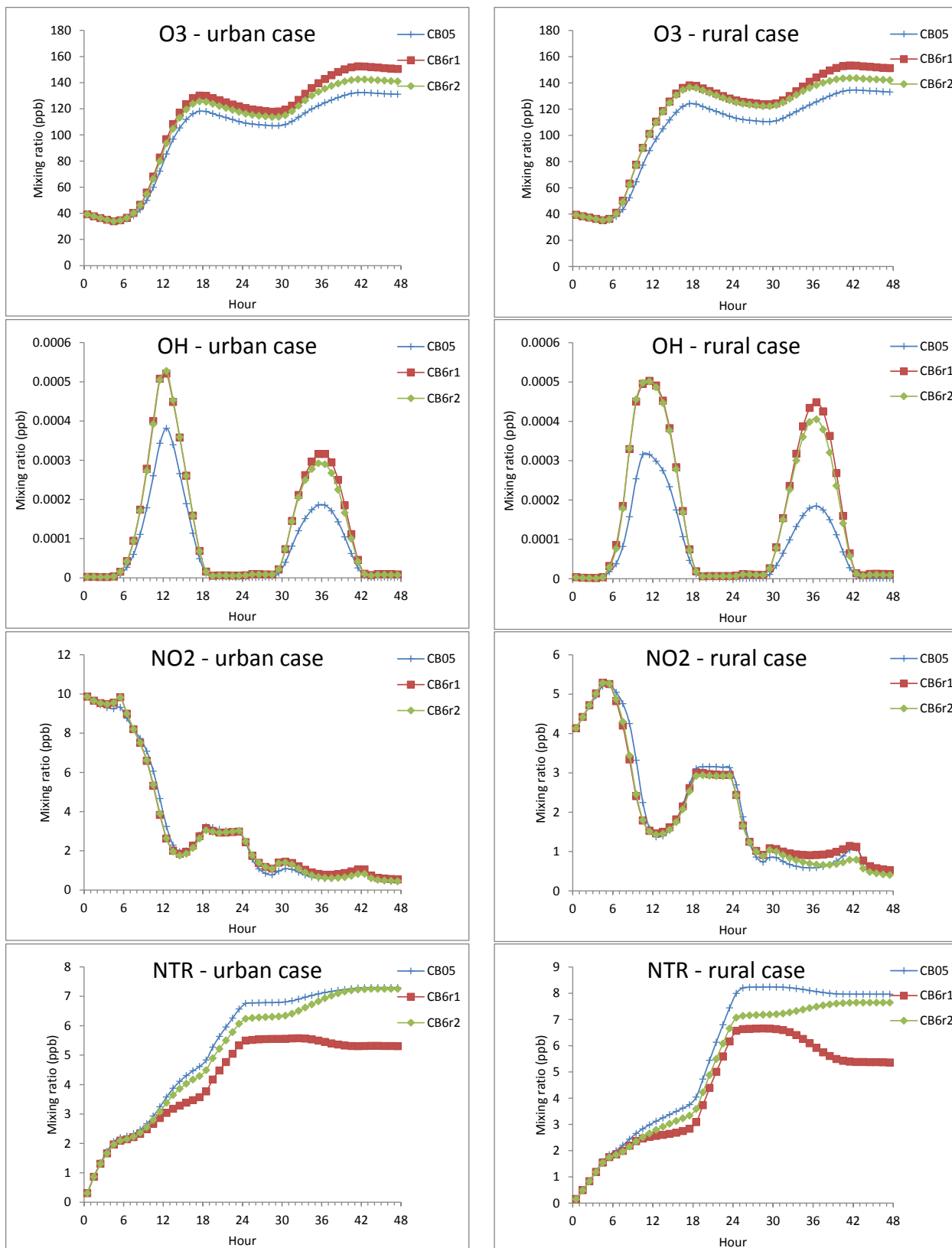
Figure 2-1. Time series of O3, OH, NO2 and NTR for box model tests with CB05, CB6r1 and CB6r2 for urban and rural VOC cases. For CB6r2 NTR shows the sum of NTR1 and NTR2.

The concentrations of ON species included in CB6r2 are shown along with NO_2 in Figure 2-2. Nitrocresol (CRON) concentrations are very small because CRON photolyzes rapidly. First generation isoprene nitrate (INTR) concentrations also are small even though isoprene contributes 57% of VOC emission in the rural case and 20% in the urban case. The small INTR concentration results from rapid reaction with OH (rate constant of 3.1×10^{-11} cm^3 molecule^{-1} s^{-1}). The dominant ON is NTR2, representing multifunctional ONs that can condense to aerosol, accounting for ~90% of ONs on day 2 for the urban VOC case and ~95% for the rural VOC case. The smaller contribution of NTR1 (5-10% on day 2) explains why CB6r2 has much less NO_x recycling via ON photolysis than CB6r1.
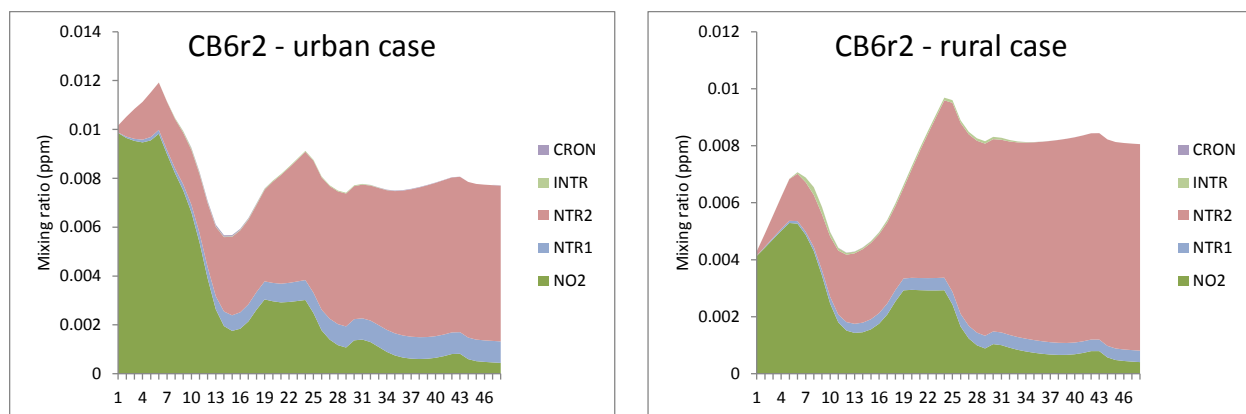
Figure 2-2. Time series of NO_2 and CB6r2 ONs (NTR1, NTR2, INTR, CRON) in box model tests for urban and rural VOC cases.

2.4 CAMx Modeling

Regional photochemical modeling was performed with CAMx (ENVIRON, 2013) using two modeling databases for different purposes. First, modeling with the TCEQ's June 2006 "Rider 8" model was performed to compare the predicted NOy composition in the free troposphere to observations from the INTEX-A field study (Singh et al., 2006). The Rider 8 model is not ideal for evaluating O_3 model performance with CB6r2 because it does not include OA and therefore the NTR2 hydrolysis was simplified to a constant rate of 2 day^{-1}. Additional CAMx modeling was performed using a database from EPA's 2005 "CSAPR" modeling that which includes OA. The CSAPR modeling was used to evaluate modeled O_3 concentrations with CB6r2.

The most comprehensive source of NOx measurements in the free troposphere over the eastern U.S. is aircraft flight data from the Intercontinental Chemical Transport Experiment A (INTEX-A) field study (Singh et al., 2006). In 2004, the INTEX-A field study was held in the U.S. under the auspices of International Consortium for Atmospheric Research on Transport and Transformation (ICARTT). Several aircraft flew missions over North America and the Atlantic and Pacific Oceans. The NASA DC-8 aircraft flew 18 missions over North America during July 1-

August 15, 2004 and measured trace gases in the troposphere and lower stratosphere from 0.2-12 km (Singh et al., 2006, 2007). The 1-minute average DC-8 measurements were provided to ENVIRON by Barron Henderson (personal communication, 2012) and were used to evaluate CAMx model performance in simulating trace gases through the depth of the troposphere in a project for TCEQ (Kemball-Cook et al., 2013). Although the INTEX-A experiment does not overlap the June 2006 Rider 8 episode, we used this data to compare the mean measured state of the atmosphere with that predicted by CAMx. We do not expect the model to exactly reproduce the INTEX-A measurements, but do expect the mean modeled NOy concentrations in the free troposphere between 3 and 5 km to agree in approximate magnitude with the measured NOy concentrations, given that the flights and modeled episode both occur during summer over the same geographic region. The height range 3 to 5 km was selected because ON concentration data are available in this range.

ENVIRON downloaded the modeling inputs from the TCEQ's Rider 8 modeling website (http://www.tceq.texas.gov/airquality/airmod/rider8) and added lightning and aircraft NOx emissions to improve model predictions for NOy in the free troposphere as described by Kemball-Cook et al. (2013).

Speciated NO_y concentrations (ppt) modeled using CAMx with CB6r1 and CB6r2 are compared to observations from INTEX-A aircraft flights between 3 and 5 km altitude in Figure 2-3. The classification of species for Figure 2-3 is as follows. PAN (peroxyacetyl nitrate), NO_2 and HNO_3 are uniquely identified in the INTEX-A data and the chemical mechanisms. PAN > C2 is the sum of PAN analogs from the INTEX-A data that are represented as PANX in the chemical mechanisms. RNO_3 in the INTEX-A data is the sum of individual alkyl nitrates (C1 to C5) quantified by GC and is comparable to NTR1 in CB6r2. X-RNO3 in the INTEX-A data is the sum of all ONs less RNO_3 and is comparable to NTR2 in CB6r2. CB6r1 has only the single species NTR which is considered most comparable to X-RNO_3. The following findings are drawn from Figure 2-3:

- RNO_3 (i.e., NTR1) constitutes ~9% of total ONs in the INTEX-A data as compared to ~21% with CB6r2 which is considered good agreement considering uncertainty in matching species definitions between CB6r2 and the INTEX-A data.
- Hydrolysis of NTR2 in CB6r2 lowers the total ON concentration by ~21% compared to CB6r1 and improves agreement with INTEX-A total ON (sum of RNO_3 and X-RNO_3) by reducing 26% over prediction with CB6r1 to 12% with CB6r2.
- Hydrolysis of NTR2 in CB6r2 raises the HNO3 concentration compared to CB6r1 and improves agreement with INTEX-A total ON by reducing 21% under prediction with CB6r1 to <1% with CB6r2.

Overall, CB6r2 improved the agreement with INTEX-A data compared to CB6r1. The CB6r2 split between NTR1 and NTR2 is in reasonable agreement with the INTEX-A data.
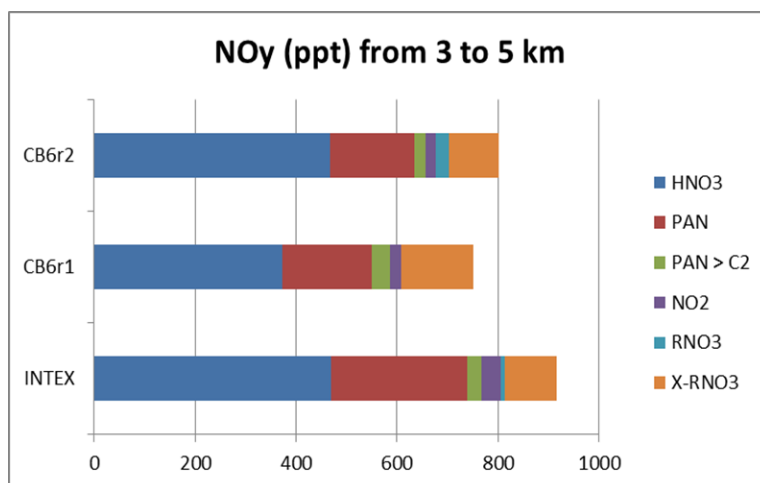
Figure 2-3. Comparison of speciated NOy concentrations (ppt) modeled using CAMx with CB6r1 and CB6r2 against observations from INTEX-A aircraft flights between 3 and 5 km altitude. The species naming is explained in the text.

Model performance for O_3 was evaluated for June 2005 with modeling based on EPA's Cross-State Air Pollution Rule (CSAPR) database (EPA, 2011). The modeling domain consists of a 36-km horizontal grid covering the entire continental U.S. and a 12-km nested grid covering most of the eastern U.S. (Figure 2-4.) Meteorological conditions and biogenic emissions were updated using the Weather Research and Forecasting (WRF) model version 3.4 (Dudhia, 2012) and the Model of Emissions of Gases and Aerosols from Nature (MEGAN) version 2.1 (Guenther et al., 2012), respectively. CAMx version 6 was used with the CB05 (Yarwood et al., 2005) CB6r1 and CB6r2 mechanisms.

Figure 2-4 shows the modeled daily maximum 8-hour average (DMA8) O_3 averaged over the month of June with the CB05, CB6r1 and CB6r2 mechanisms. Modeled O_3 with CB6r1 is higher than with CB05 which, from the box modeling results discussed above, can be attributed to (1) greater ozone production from fresh emissions with CB6r1 and/or (2) greater NO_x recycling from ONs leading to more O_3 production as emissions are processed at regional scale. An O_3 difference plot for CB6r1-CB05 shown in Figure 2-5 shows that the O_3 increases with CB6r1 are regional in nature suggesting that greater NO_x-recycling in CB6r1 is the dominant cause of O_3 increases over CB05. Modeled O_3 with CB6r2 is lower than with CB6r1 and this reduction must be attributable to the revised ON scheme in CB6r2 reduced the amount of NO_x recycling from ONs. The O_3 difference CB6r2-CB05 in Figure 2-5 shows that CB6r2 produces more ozone (monthly average DMA8) than CB05.
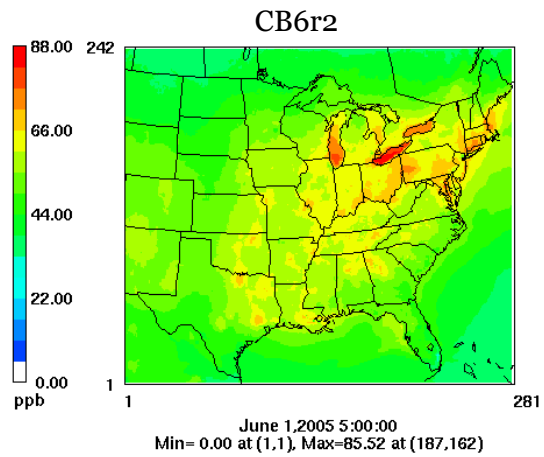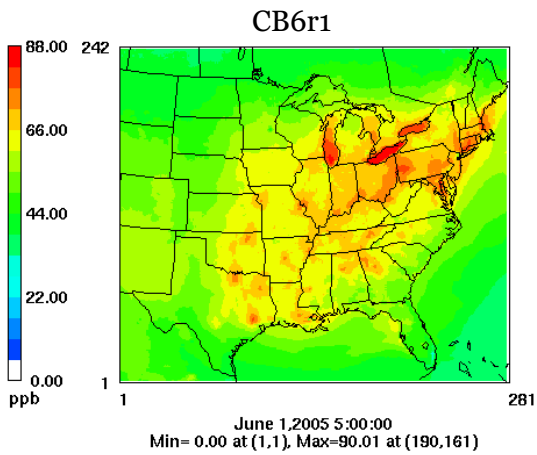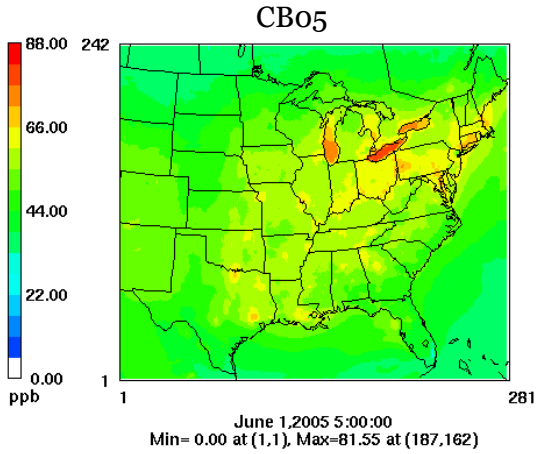
Figure 2-4. Monthly averaged DMA8 O3 (ppb) for June 2005 in the CSAPR model.
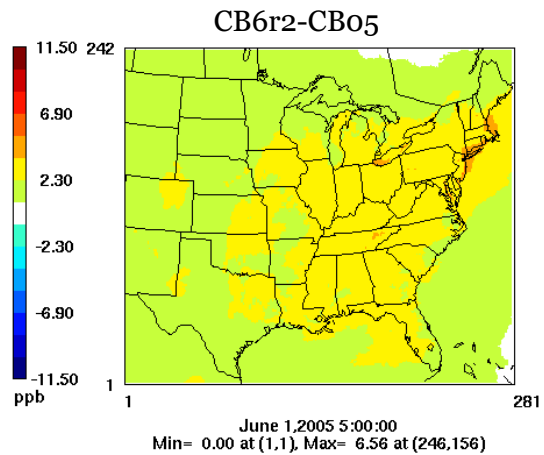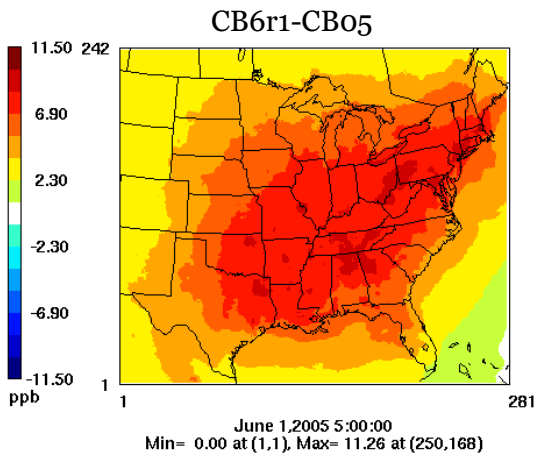

Figure 2-5. Differences in monthly averaged DMA8 O3 (ppb) for June 2005 in the CSAPR model.

Model performance was evaluated statistically by computing model fractional bias and error:

$$\text{Fractional Bias (FB)} = \frac{2}{N} \sum_{i=1}^{N} \left(\frac{P_i - O_i}{P_i + O_i} \right)$$

$$\text{Fractional Error (FE)} = \frac{2}{N} \sum_{i=1}^{N} \left| \frac{P_i - O_i}{P_i + O_i} \right|$$

Where P_i and O_i are predicted and observed values at the i-th monitoring site, respectively, and N is the number of monitoring sites. Hourly observation data were from EPA's extensive Air Quality System (AQS) network of monitoring sites that are predominantly in urban areas and from the Clean Air Status and Trends Network (CASTNET) operated by EPA and the National Park Service for monitoring long-term O_3 trends in rural areas. The evaluation was performed for each of four U.S. Regional Planning Organization (RPO) regions in the eastern US: Central Regional Air Planning Association (CENRAP), Midwest Regional Planning Organization (MRPO), Mid-Atlantic/Northeast Visibility Union (MANE-VU), and Visibility Improvement State and Tribal Association of the Southeast (VISTAS).

Fractional bias is shown in Figure 2-6 and compared to a performance objective of +/- 15% whereas fractional error is shown in Figure 2-7 and compared to a performance objective of 35%. CB6r2 has smaller error than CB6r1 for all regions and both networks. CB6r2 has smaller bias than CB6r1 in all regions except CENRAP where CB6r1 over predicted and CB6r2 under predicts. CB6r2 meets the bias performance objectives for all regions and networks whereas CB6r1 exceeds the bias objective in the VISTAS and MANE-VU regions for both networks. CB6r2 clearly improves model performance for O_3 over CB6r1 in the MANE-VU, Midwest RPO and VISTAS regions, and in the CENRAP region CB6r1 and CB6r2 perform about equally well. Comparing CB6r2 with CB05, both mechanisms perform about equally well overall and meet all performance objectives, with CB05 doing slightly better in the MANE-VU and VISTAS regions and CB6r2 doing slightly better in the Midwest RPO region.
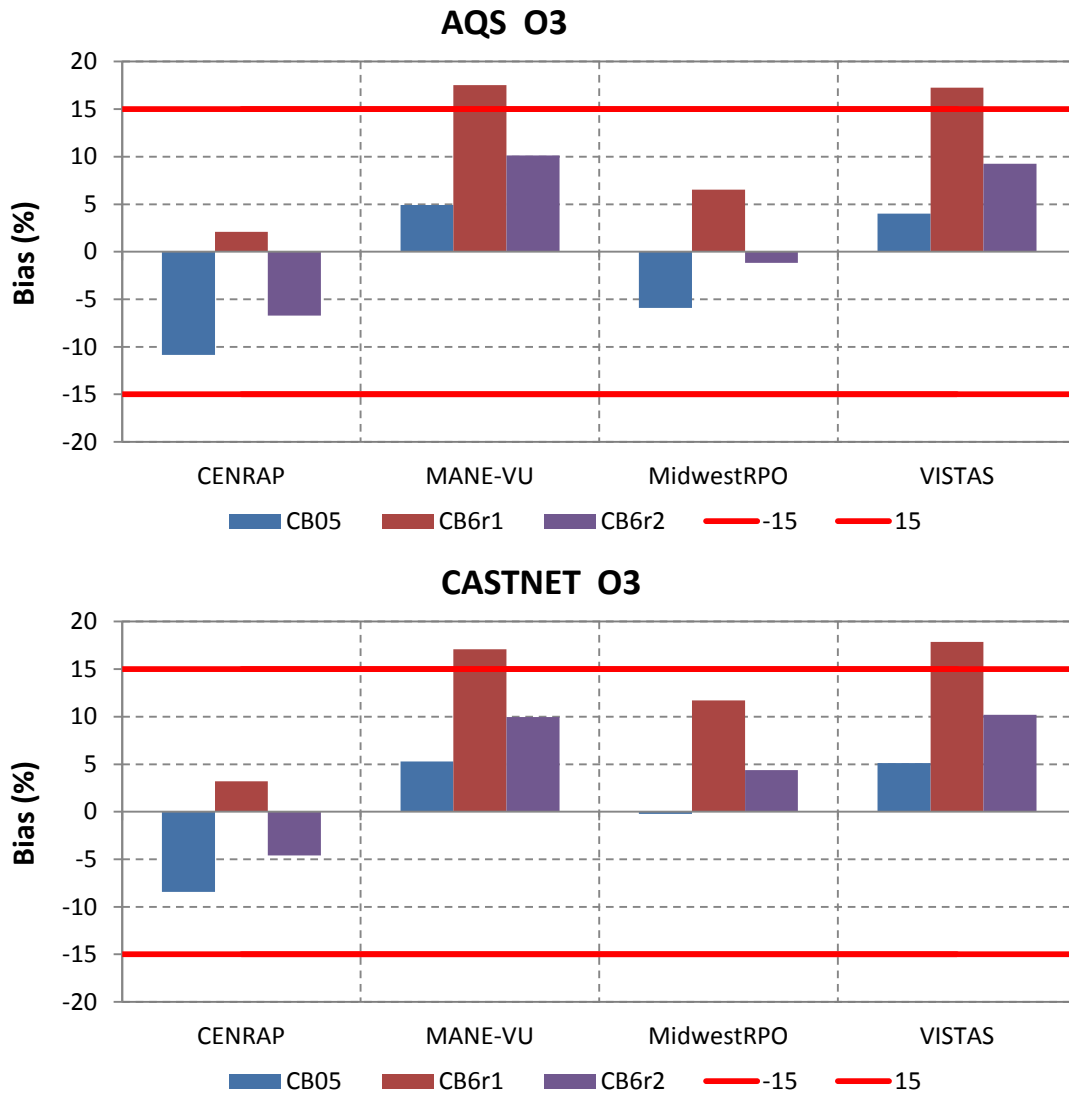
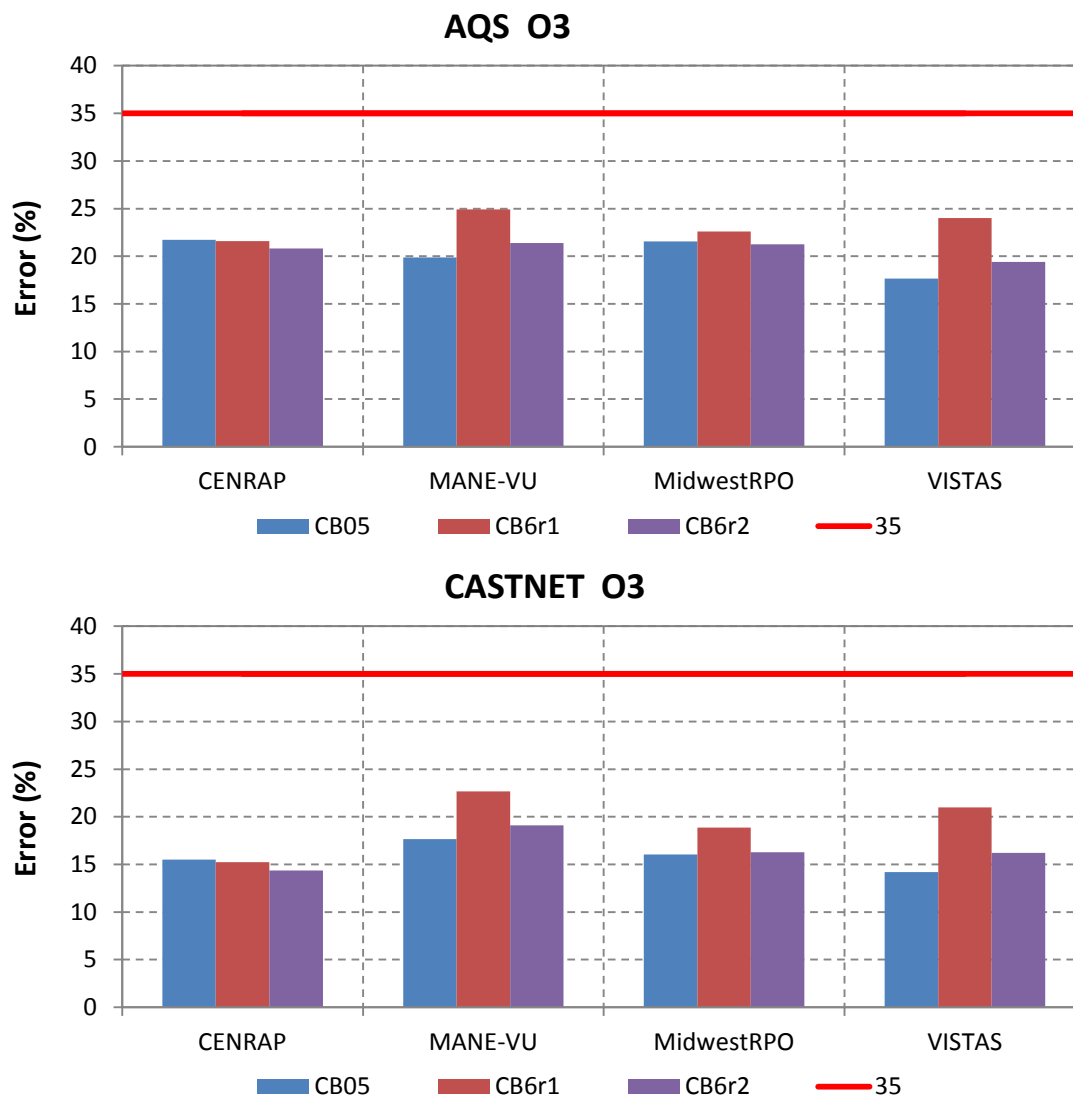**Figure 2-6. Fractional bias (%) in O3 for June 2005 in the CSAPR model.**

Figure 2-7. Fractional error (%) in O$_3$ for June 2005 in the CSAPR model.

2.5 Recommendations

Uncertainty in the atmospheric fate of ONs adds substantial uncertainty in modeling regional O$_3$ and other oxidants. Additional laboratory studies and ambient measurements are needed to better quantify partitioning of ONs to aerosol, forming ANs, and the subsequent chemical fate of ANs.

The ON scheme implemented in CB6r2 is simple and generally consistent with available studies and improves the performance of CB6r2 in simulating regional O$_3$ and NOy speciation compared to CB6r1. CB6r2 is recommended over preceding versions of CB6.

CB05 continues to perform well in simulating regional O_3 in large part because of the way that ONs (CB05 species NTR) are represented. The reaction of OH with NTR inCB05 forms HNO_3 which could be considered to be a highly condensed version of the CB6r2 ON scheme. While CB05 performs well for regional O_3, it predicts much lower OH concentrations than CB6r2 in large part because the CB05 isoprene mechanism is dated. Use of CB6r2 is preferred over CB05.

3.0 Laboratory Experiments

UT-Austin conducted laboratory chamber experiments in a new environmental chamber, which is a ~ 10 m^3 Teflon bag suspended inside of a temperature-controlled room, similar to the chamber previously used by Yarwood et al. (2012). The walls of the room are lined with UV lights which enable the production of photochemical oxidants and the simulation of photochemical reactions.

3.1 Experimental Procedures

Before every experiment the chamber was flushed and then filled with clean air generated using an Aadco clean air generator (Model 737-14A). In most PM formation experiments (Experiments 1 through 8, Table 3-1), inorganic seed particles were then injected which were formed from aqueous solutions of ammonium sulfate $((NH_4)_2SO_4)$. The seed particles serve as surface area onto which organic vapors can condense, and they also aid in correcting the data for particle loss to the chamber walls. A hydroxyl radical precursor was then injected – either HONO, which photolyzes to form OH and NO, or H_2O_2 which photolyzes to 2OH. When H_2O_2 was used, NO_2 was also injected so that experiments were conducted in the presence of NO_x. Finally, a volatile organic compound (VOC) was injected. When all compounds were well mixed, the UV lights were turned on, starting the formation of the OH radical, the oxidation of the VOC and the formation of organic nitrates and other oxidized organic species. The experimental conditions of experiments 1 – 8 are summarized in Table 3-1. The relative humidity in all experiments was less than 5%.

Two additional experiments (Experiments 9-10, Table 3-2) were conducted in which α-pinene was photo-oxidized in the presence of isobutyl nitrate (Experiment 9) or nitropropane (Experiment 10). In these experiments the small organic nitrogen molecule served as a NO_x source. Experimental conditions for these two experiments are summarized in Table 3-2.

Table 3-1. Conditions and particulate mass formed in experiments 1-8.

Expt. #	VOC	OH precursor	Seed Particles	$[VOC]_0$ (ppb)	$[NOx]_0$ (ppb)	Temp (°C)	PM NO_x ($\mu g\ m^{-3}$)*	PM Org. ($\mu g\ m^{-3}$)*
1	toluene	HONO	no	190	N/A	25	5	26
2	toluene	HONO	yes	190	N/A	20	2	6
3	isoprene	H_2O_2	yes	200	48	30[a]	12	76
4	toluene	H_2O_2	yes	190	34	20	7	63
5	isoprene	HONO	yes	200	700	20	2	9
6	n-decane	H_2O_2	yes	100	54	25	4	52
7	o-cresol	HONO	yes	200	18	25	5	120
8	isoprene	HONO	yes	200	40	20	1	5

[a] temperature control failed during this experiment

* measured after 1 hour of photo-oxidation

Table 3-2. Conditions and particulate mass formed in experiments 9-10.

Expt. #	VOC	Org. Nitrate	$[VOC]_0$ (ppb)	$[Org\ Nitrate]_0$ (ppb)	Temp (°C)	PM NO_x ($\mu g\ m^{-3}$)[b]	PM Org. ($\mu g\ m^{-3}$)[b]
9	α-pinene	isobutyl nitrate	60	90	20 then 40	2	80
10	α-pinene	nitropropane	60	110	20,40,20	3	130

3.1.1 Instrumentation

Concentrations of gas- and particle-phase species were monitored throughout the experiments using state-of-the-art instrumentation. The High-Resolution Time-of-Flight Chemical Ionization Mass Spectrometer (HRToF-CIMS) can measure the molecular composition and concentration of species in the gas phase (Bertram et al., 2011; Yatavelli et al., 2012) . For these experiments the instrument was operated using water clusters ($H_3O^+ \bullet (H_2O)_n$) as chemical ions. In this mode the instrument can detect organic nitrogen compounds and other hydrocarbons, including most precursor VOCs as well as moderately functionalized oxidation products. Water cluster chemical ionization is similar but not equivalent to proton transfer reaction - mass spectrometry (PTR-MS); the higher proton affinity of $H_3O^+ \bullet (H_2O)_n$ compared to just H_3O^+ results in more selective ionization which does not ionize species of zero dipole moment. Other gas-phase measurements included concentrations of O_3 and NO_x using standard chemiluminescence - based monitors from Teledyne instruments (models 400E and 200E for O_3 and NO_x, respectively). Concentrations of NO_2 were also measured using an NO_2 monitor from Environnement (Model AS32M), which uses Cavity Attenuated Phase Shift (CAPS) technology to obtain a direct NO_2 measurement (Kebabian et al., 2008). Unlike the chemiluminescence-based

monitors, the CAPS NO_2 monitor does not convert all nitrogen-containing species to NO and is therefore not sensitive to other nitrogen-containing compounds such as organic nitrates or HONO.

Particle-phase composition was monitored using an Aerosol Chemical Speciation Monitor (ACSM) from Aerodyne, Inc. which provides mass concentrations of sulfate, ammonium, nitrate and organics in PM_1. In the ACSM particles are flash vaporized when they impact a heater, and the resulting molecules are ionized by electron-impact ionization. This method of ionization is relatively harsh resulting in fragmentation of molecules. The molecular fragments are then later attributed to the different bulk species using a fragmentation table (Allan et al., 2004a); adjustments made to the standard fragmentation table are described in section 3.1.2 below. The ACSM was operated to automatically alternate between a "filter" mode in which particles are removed from the sample air before they are sent to the ACSM, and a "sample" mode, in which the particles are not removed from the air before it is sent to the ACSM. The averaging time of the instrument (one filter-sample cycle) was set to 2.5 min. The vaporizer temperature was set to the standard 600°C to ensure fast and complete vaporization of ammonium sulfate. The AMS measures only non-refractory (NR) PM_1, i.e. compounds that flash-vaporize at 600°C.

In addition to particle composition, particle size distributions were also measured using a Scanning Electrical Mobility Spectrometer (SEMS) from Brechtel Manufacturing, Inc. This instrument consists of two main parts: a Differential Mobility Analyzer (DMA), which size-selects airborne particles based on their electric mobility, and a condensation particle counter (CPC), which counts the particles. As the DMA scans through different voltages, particles of different sizes pass through the DMA and are counted in the CPC. By scanning through different voltages, the instrument is able to provide measurements of the particle size distribution. The set-up of instrumentation used in the environmental chamber experiments is shown in Figure 3-1.
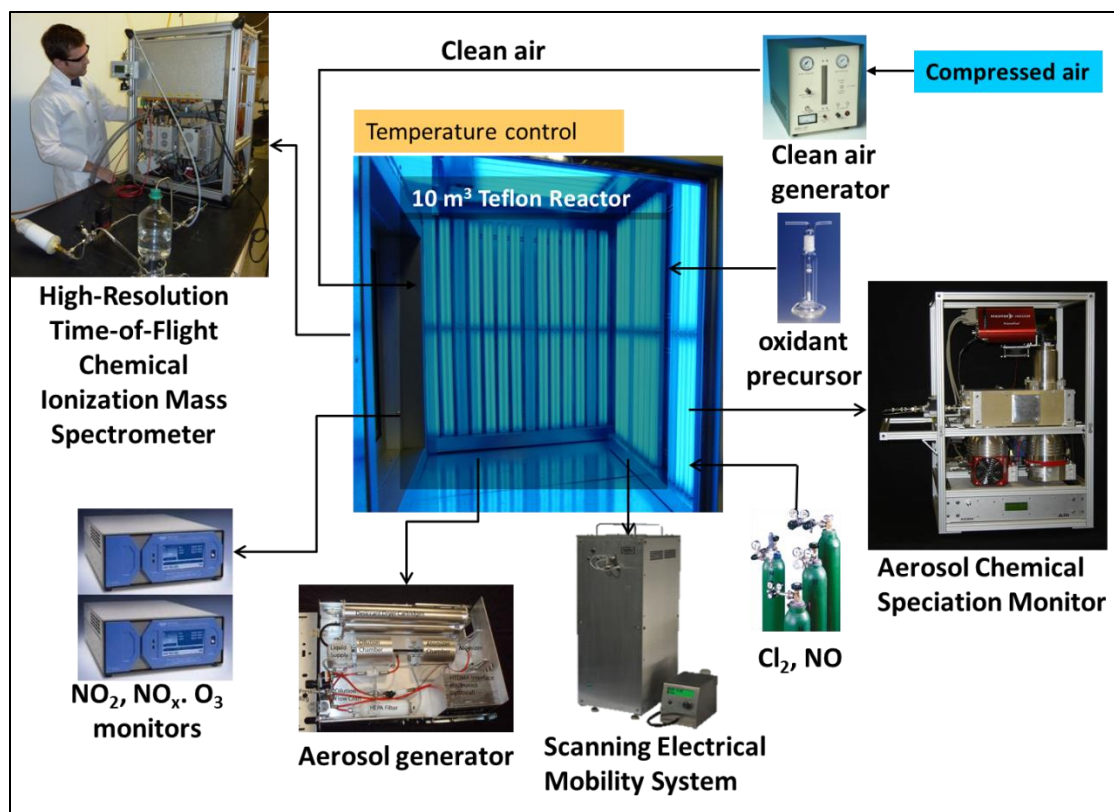
Figure 3-1. Set-up and instrumentation used in laboratory chamber experiments.

3.1.2 Data Analysis

3.1.2.1 HRToF-CIMS data analysis

Mass spectrometer data from the HRToF-CIMS were saved in hierarchical data format (hdf) by the data acquisition software provided by the manufacturer. The data were processed using the data analysis software "Tofware", provided by the manufacturer and written in Igor Pro (Wavemetrics). The functions in Tofware include a correction for the ToF duty cycle, a mass calibration based on selected known ions, interpolation and subtraction of the baseline, and determination of the resolution and shape of the ion peaks. The signal is then integrated - either all signal at a nominal mass to charge ratio (m/z) for unit mass resolution (UMR) analysis or each individual ion peak for high resolution (HR) analysis.

All data were analyzed in high resolution, which means that multiple peaks were found at a given integer m/z value. Peaks up to m/z 300 were found using Tofware's HR browser using an averaged spectrum. However, peaks above m/z 200 typically have many potential fits due to the high number of atoms per molecule so only high magnitude peaks in the range above m/z 200 were fit. These peaks were then integrated for each mass spectrum over the time of the

experiment. Analyte signals were normalized by the sum of the reagent ion signals at *m/z* 19, 37, and 55 (H_3O^+, $H_3O^+\bullet$ (H_2O), and $H_3O^+\bullet$ (H_2O)$_2$ respectively) to account for possible variation in instrument sensitivity. A calibration curve (when available) could then be fit to this normalized signal.

3.1.2.2 ACSM data analysis

Data from the ACSM were analyzed using the data analysis software "ACSM Local" provided by the manufacturer and written in Igor Pro. In addition to calculating and displaying the chemically speciated aerosol mass loadings, ACSM Local has tools for examining the ACSM data stream in detail and monitoring instrument performance. Particles can bounce on the vaporizer resulting in a collection efficiency (CE) of less than 1. ACSM data were simultaneously corrected for CE and chamber wall losses by assuming that all particles lost to the walls are able to participate in gas-particle partitioning as if they were in suspension. This assumes that there are no mass transfer limitations to gas-particle partitioning close to the chamber walls. If this is the case, the ratio of organics (including organic nitrates) to ammonium sulfate should remain the same for suspended and wall-deposited particles, and corrected mass concentrations of organics and organic nitrates were obtained by multiplying the ratio of organics to ammonium sulfate by the initial ammonium sulfate concentration, as has been done in previous work (Hildebrandt et al., 2009). By using the initial ammonium sulfate concentration measured by the SEMS, which is not prone to uncertainties due to the ACSM collection efficiency, we simultaneously correct for the ACSM collection efficiency and particle wall loss rates. The (NH_4)$_2SO_4$ signal was smoothed by using a binomial smoothing algorithm in Igor Pro.

For the case in which no data on (NH_4)$_2SO_4$ were available (Experiment 1), data were only corrected for collection efficiency based on the difference between the total mass measured by the ACMS and the total mass measured by the SEMS; the collection efficiency thus obtained was 0.5. Total volume concentrations from the SEMS were converted to total mass concentrations using the ACSM data to calculate a time series of density, assuming a density of 1.4 kg/m^3 for organics and organic nitrates and 1.77 kg/m^3 for ammonium sulfate.

Adjustments to standard fragmentation table

The fragmentation patterns of air, water and organics were evaluated using the filter measurements which are taken throughout each experiment. For air, the fragmentation pattern at *m/z* 44 (CO_2^+), *m/z* 29 ($N^{15}N^+$) and *m/z* 16 (O^+) was measured and adjusted, as is customary. $N^{15}N^+$ and CO_2^+ were calculated as fractions of the N_2^+ signal at *m/z* 28. O^+ was calculated as a fraction of N^+ at *m/z* 14. The water fragmentation pattern at *m/z* 16 (O^+), *m/z* 17 (OH^+) and *m/z* 18 (H_2O^+) was determined by calculating the ratios of *m/z* 16 and m/z 17 versus *m/z* 18. In addition to the water fragmentation, the ratio of water H_2O^+ to N_2^+ was also determined, which depends on ambient humidity.

For the organic fragmentation pattern we used the recommendation by Aiken et al. (2008) that m/z 28 = 100% × m/z 44; in the original AMS fragmentation table this was set to 0%. However, differently from the recommendation of Aiken et al. (2008) we retained the ratio of m/z 18 to m/z 44 as 100%; the new recommendation was to set this ratio to 22.5%. The reason we change this was because recent work has shown that a m/z 18 / m/z 44 ratio of 100% is more consistent with data and with calibration experiments (M. Canagaratna , personal communication).

3.1.2.3 Other instruments

Data from the Scanning Electric Mobility Spectrometer (SEMS) were also processed by the data analysis software provided by the manufacturer which "inverts" the data from units of number vs. voltage to number vs. particle mobility diameter (Dm), resulting in a particle size distribution. The software also corrects the data for multiply charged particles (assuming a Boltzmann charge distribution) and accounts for diffusion. The data are then read into and displayed in Igor Pro. Data from the NO_x, NO_2 and O_3 monitors were saved in time-stamped delimited text formats. These data did not need additional processing. The instruments were calibrated using a 5-point calibration before this set of experiments was started.

3.2 Experimental Results

3.2.1 Evolution of VOCs, NO_x and Ozone

Figure 3-2 below shows the concentrations of the precursor VOC, NO_x and ozone for experiments 3-8. The NO_x and NO_2 monitors were not available for experiments 1 and 2. The HRToF-CIMS is not sensitive to decane (Expt. 6), and measurements of o-cresol (Expt. 7) were also not successful. In all experiments, NO_x concentrations decrease and ozone concentrations increase as the VOC is photo-oxidized in the presence of NO_x, confirming that reactions of VOCs + NO_x are an ozone source and NO_x sink.
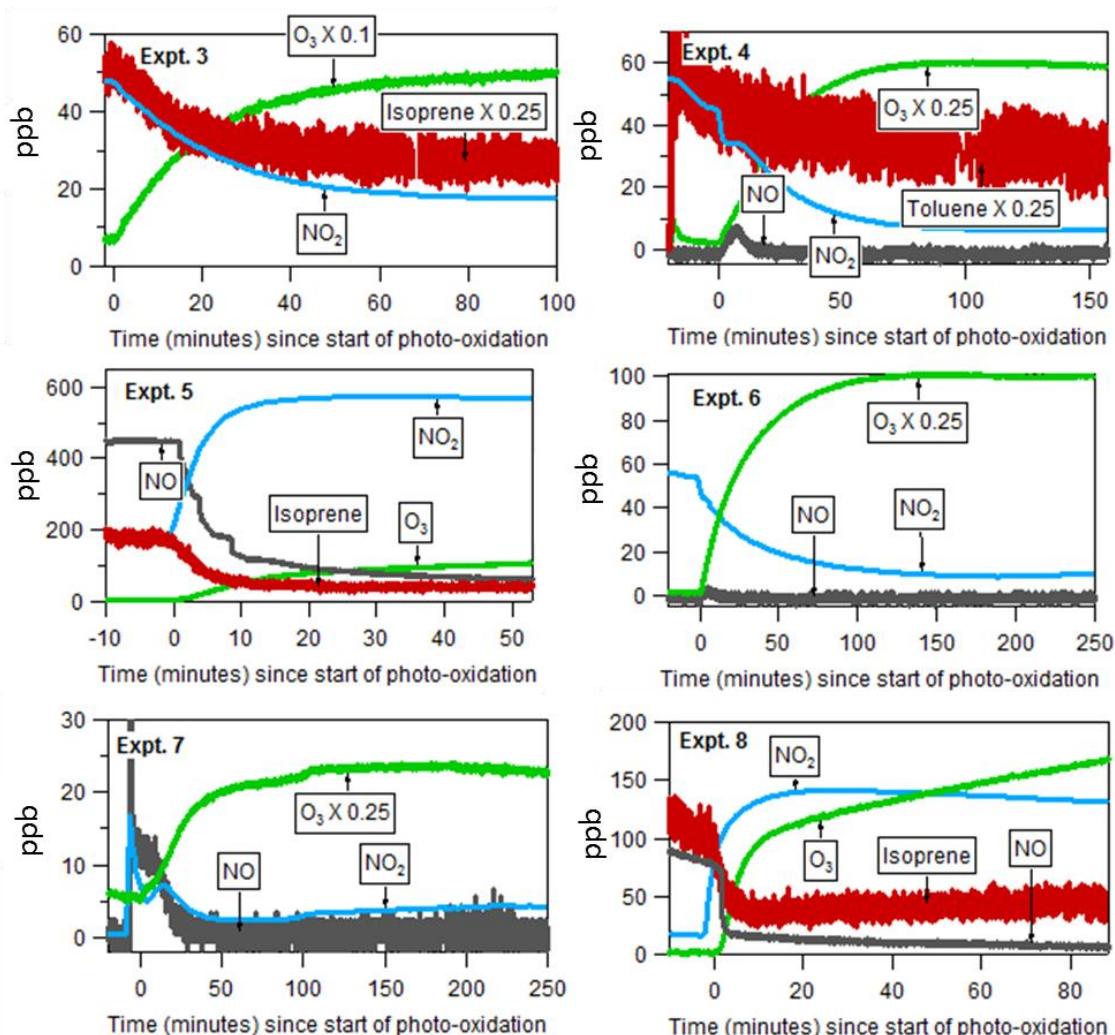
Figure 3-2. Concentrations of VOCs, NO$_x$ and ozone in experiments 3-8 confirm that reactions of VOCs and NO$_x$ are an ozone source and NOx sink.

3.2.2 Formation of Gas-Phase Organic Nitrates

Figure 3-3 below shows the concentrations of the organic nitrogen (ON) species detected in the gas-phase during experiments 1-10; in all experiments, significant formation of gas-phase organic nitrates was observed. For each experiment only the most abundant ON are plotted. Due to differences in sensitivity to different species in the HR-ToF-CIMS only the normalized signal (analyte signal divided by reagent ion signal) is plotted; more detailed calibration experiments are underway. In the toluene and o-cresol photo-oxidation experiments the molecular formulas of the most abundant ON were consistent with nitro-toluene ($C_7H_7NO_2^+$) and methyl-nitrophenol ($C_7H_7NO_3^+$); our analysis methods only yield molecular formulas; we cannot distinguish between isomers. Nitrotoluene forms when the methyl

29

hydroxycyclohexadienyl radical reacts with NO_2. The radical could also react with O_2 to form cresol, and based on the rate constants of these reactions the formation of nitro-toluene is expected to be significant only at NO_2 concentrations exceeding 300 ppb (Seinfeld and Pandis, 2006). The concentrations of NO_x in our experiments were always below 100 ppb, so the significant formation of nitro-toluene or any other $R-NO_2$ compounds is surprising and is subject of ongoing work.

In isoprene photo-oxidation experiments the most abundant ON signals were $C_5H_{14}NO_3^+$ and $C_4H_8NO_3^+$. In most cases the HRToF-CIMS works through proton transfer ionization but in the case of $C_5H_{14}NO_3^+$ this would imply an analyte molecule with too many hydrogen atoms. We hypothesize that in this case the observed ion is the cluster $C_5H_{11}NO_2 \cdot H_3O^+$. This cluster of H_3O^+ with compounds as opposed to the simple transfer of H^+ was seen in other, less abundant compounds as well. The other compound ($C_4H_7NO_3^+$) could be the result of ON formation from an isoprene photo-oxidation product such as methyl vinyl ketone or methacrolein. The most abundant compounds formed in the photo-oxidation of n-decane all retain their original carbon backbone; all of the ONs observed in this experiment are multifunctional ONs.

3.2.3 Formation of Particle-Phase Organic Nitrates

As demonstrated in section 3.2.2 above, organic nitrogen compounds were formed in all PM formation experiments (1-8). A significant fraction of the organic nitrates partitioned to the particle phase. Figure 3-4 shows the time series of particulate NO_x (the mass of NO^+ and NO_2^+ fragments measured by the ACSM) and particulate organics formed in each of the eight experiments. Table 3-1 summarizes the mass of NO^+ and NO_2^+ (NO_x) fragments and total organics found in the particle phase after 1 hour of photo-oxidation; it also notes initial concentrations of VOCs and NO_x for all experiments.

Organic nitrogen molecules fragment in the ACSM into NO^+ or NO_2^+ and an organic fragment. The total organic nitrate mass from the ACSM is therefore a sum of the mass attributed to NO^+ and NO_2^+ ('particulate NO_x' in Figure 3-4) and some portion of the mass attributed to organics. Even if we assume a relatively low molecular weight of the organic nitrogen molecules (~ 100-150 amu), in most experiments over half of the total organic mass is composed of organic nitrogen molecules. There is some correlation between the ratio of initial NO_x/VOC and PM-NO_x/PM-Organics; for example, experiment 7, which exhibited the lowest initial NO_x/VOC also exhibited the lowest PM-NO_x/PM-Organics. However, there are certainly other factors such as the VOC precursor, which seem to affect formation of PM organic nitrates. Clearly, the photo-oxidation of VOCs in the presence of NO_x results in significant concentrations of particle-phase organic nitrates.
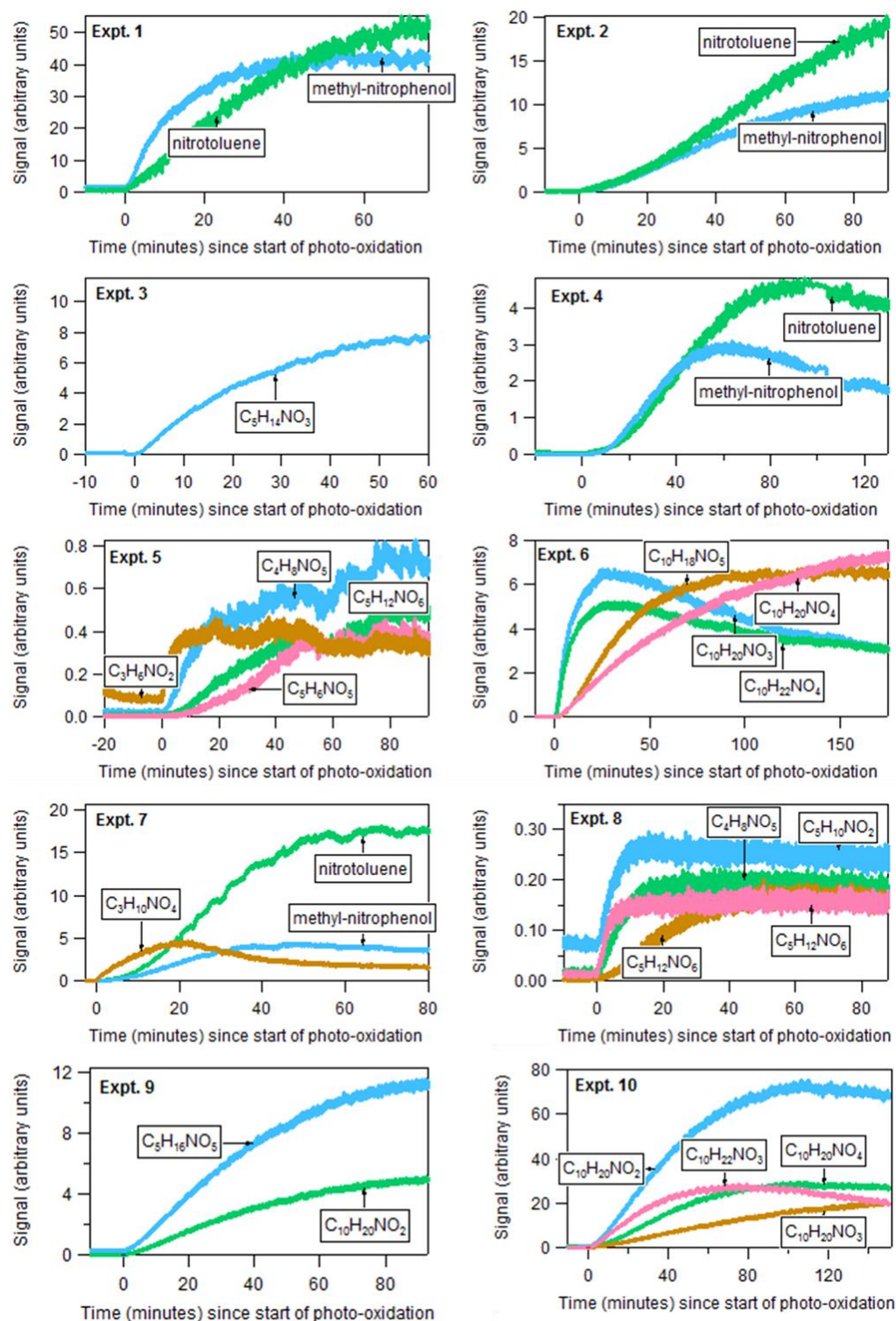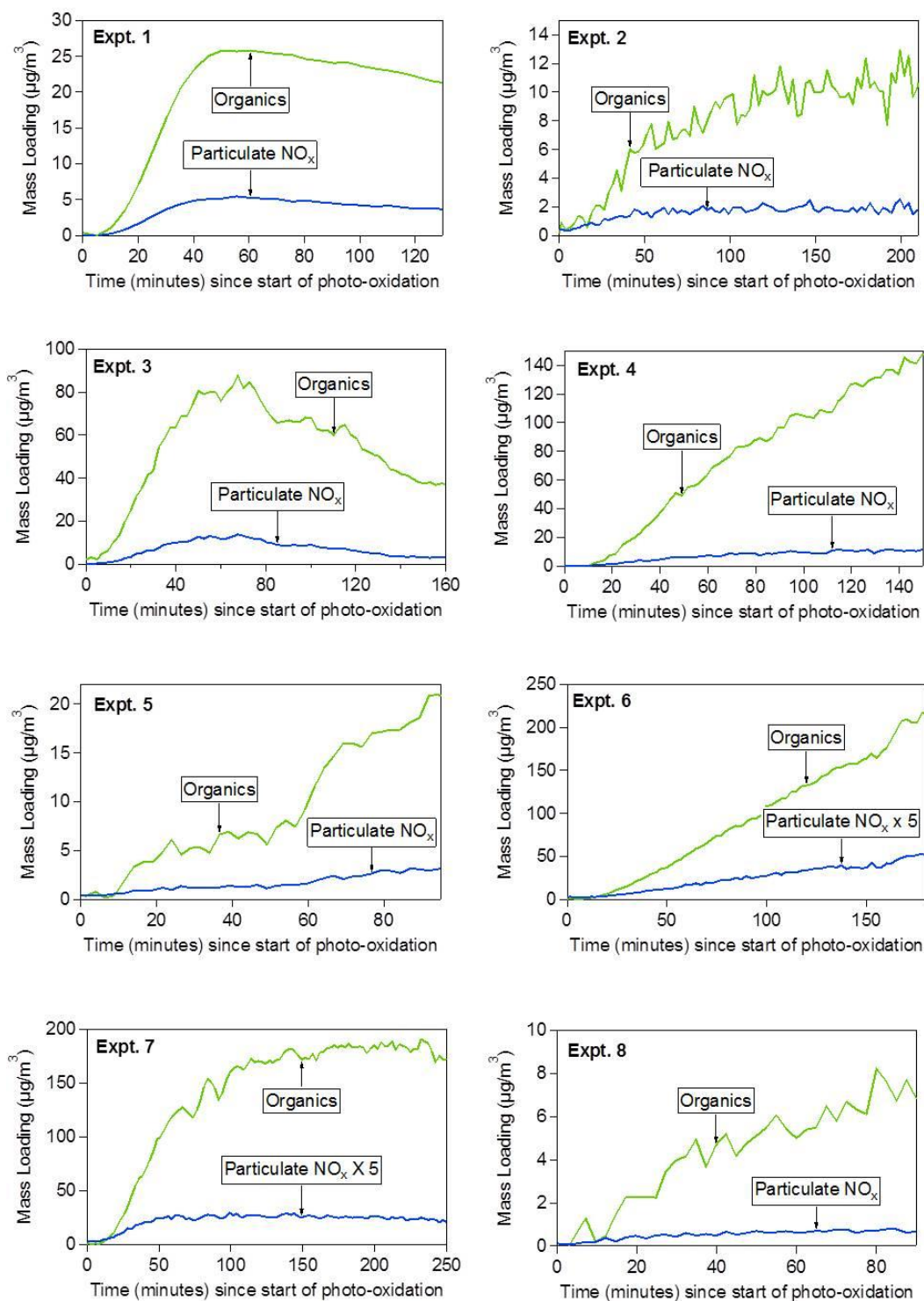
Figure 3-3. Gas-phase organic nitrogen species formed in experiments 1-10.

Figure 3-4. Particulate organic nitrates and other organics formed in experiments 1-8 as measured by the ACMS. Organic nitrogen compounds fragment in the ACMS and are detected as NO and NO$_2$ (blue trace). Particulate organics (green) are composed of fragments from organic nitrates and other organics. In each experiment, a significant amount of organic nitrates was formed and partitioned to the particle phase.

3.2.4 Gas-Particle Partitioning of Organic Nitrates

Previous work by Perraud et al. suggested that organic nitrogen compounds partition to the particle phase irreversibly (Perraud et al., 2012), which could serve as guidance on how to model the uptake of organic nitrates to the particle phase. We tested the reversibility of organic nitrate partitioning by changing the temperature inside of the environmental chamber at the end of experiment 10 and observing whether and to what extent PM-nitrates and other organics partition back to the gas-phase at higher temperatures. Figure 3-5 below shows the signal of the highest-concentration gas-phase organic nitrogen species during this experiment, as well as the temperature of the chamber. The concentration of gas-phase organic nitrates correlates with the temperature in the chamber, consistent with partitioning of the species to the particle phase at lower temperature, and partitioning back from the particle phase to the gas phase at higher temperatures.
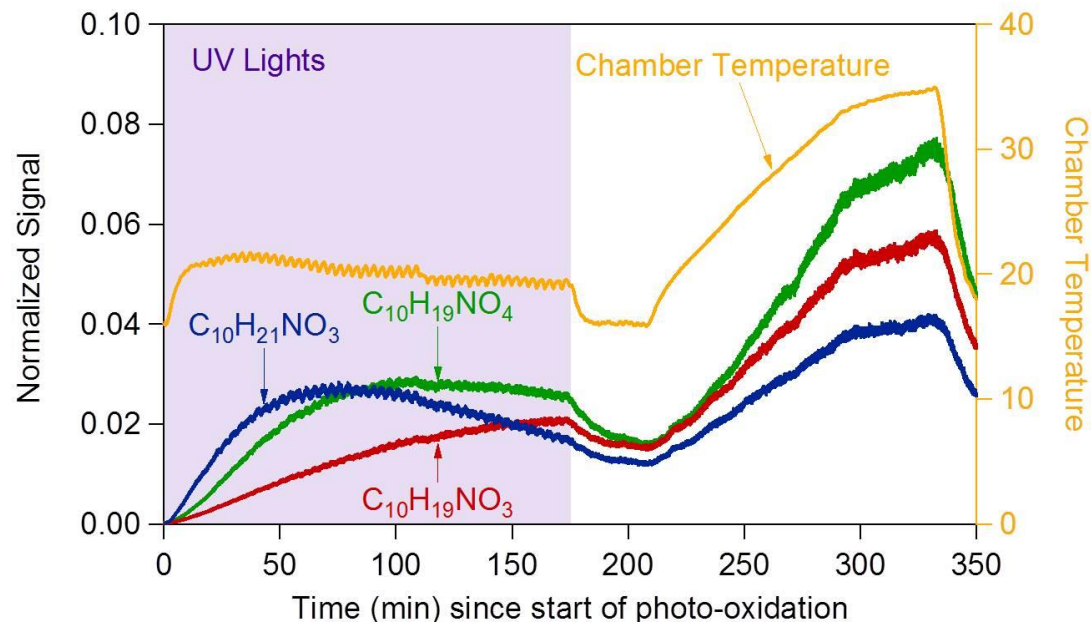
Figure 3-5. Concentration of gas-phase organic nitrogen species as the temperature in the chamber was varied at the end of experiment 10. The data are consistent with reversible partitioning of the organic nitrates: their gas-phase concentrations decrease when the chamber temperature is lower; and they increase when the chamber temperature is higher. While they UV lights are on, organic nitrogen concentrations increase as the species are formed.

When observing only the gas-phase compounds we cannot rule out that the species may partition to the chamber walls instead of the suspended particles. Figure 3-6 below shows that the particle-phase data are also consistent with gas-particle partitioning of the organic nitrates. The figure shows the ratios of PM-NO_x and other organics versus PM-Sulfate (SO_4) during experiment 10 as the temperature of the chamber was varied. Ratios to PM-Sulfate are used to

eliminate the effects of particle wall-losses, which occur throughout the experiment (PM-sulfate changes only due to wall losses in this experiment; the chamber temperature was not raised enough to cause evaporation of sulfate). Since PM-sulfate concentrations were rather low and noisy in this experiment, an exponential fit to the sulfate data was used to compute the ratios. The data show that concentrations of PM-NO$_x$ and organics decrease at higher chamber temperature, consistent with the evaporation of these species. The limited data at the end of the experiment further suggests that the concentrations of PM-NO$_x$ and organics increase when the chamber temperature is decreased. Thus, both the gas- and particle-phase data for organic nitrates and other organics suggest that these species partition readily and reversibly between the gas and particle-phases. Our data are therefore not consistent with those of Perraud et al. (2012), and it appears that the partitioning of organic nitrates should be modeled as a reversible process.
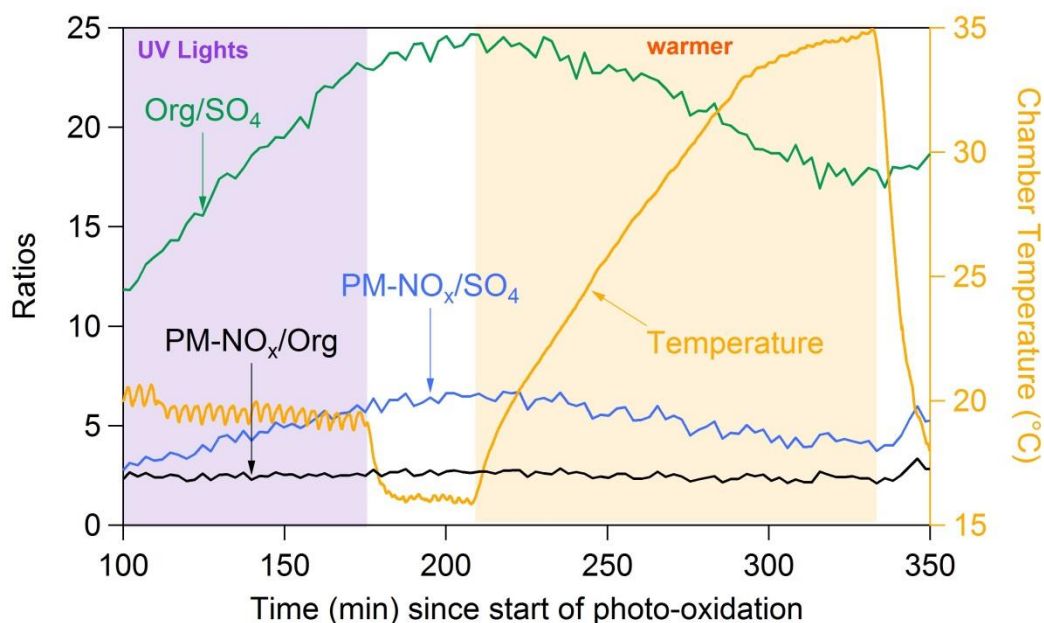
Figure 3-6. Concentration of particle-phase organic nitrogen species and other organics as the temperature in the chamber was varied at the end of experiment 10. The data are consistent with reversible partitioning of the organic nitrates and other organics to and from the particle phase.

3.2.5 Discussion of Experimental Results and Future Work

Our experiments confirm that reactions of VOCs and NO$_x$ form ozone and act as a sink for NO$_x$ (3.2.1), and a source of organic nitrogen species (3.2.2). Under typical ambient conditions a significant fraction of the organic nitrogen species is present in the particle phase (3.2.3), and the species partition readily between the gas- and particle phases (3.2.4).

34

Our understanding of the formation and fate of organic nitrates could be improved by several future experiments. These include additional experiments in which the chamber temperature is varied to explore vapor pressure of organic nitrogen species. Furthermore, all experiments in this work were conducted at low relative humidity (RH); however recent work has suggested that organic nitrogen compounds can hydrolyze in the aerosol phase at higher RH (Browne et al., 2013; Liu et al., 2012). Therefore, we also plan to conduct additional experiments at higher RH and observe the difference in the formation and fate of organic nitrates with different RH. Previous experiments on the hydrolysis of organic nitrogen (ON) compounds have focused on the hydrolysis of species formed from oxidation of tetra-methyl-benzene (Liu et al., 2012). We plan to focus our experiments on organic nitrogen species from biogenic VOCs such as alpha-pinene since these have not been explored to date and also since these VOCs were abundant in Conroe, TX, so the experiments would be beneficial to help interpret ambient data.

4.0 Ambient Measurements

During the month of September 2013 measurements were taken in Conroe, TX (EPA Site Number: 483390078) near Houston as part of DISCOVER-AQ (Deriving Information on Surface Conditions from Column and Vertically Resolved Observations Relevant to Air Quality, http://discover-aq.larc.nasa.gov).

4.1 Instrumentation and data analysis

A trailer was set up at the Conroe, TX measurement site to house the instruments used for this measurement campaign: the HRToF-CIMS, ACSM, SEMS, O_3, NO_x and NO_2 monitors. The instruments and data analysis are only described briefly here; a more detailed description was provided in sections 3.1.1 and 3.1.2. In addition to the instrumentation in our trailer, $PM_{2.5}$ filter samples were also collected at the measurement site and will be analyzed in future work. Photographs of the trailer and set-up of instruments inside of the trailer are provided in Figure 4-1 below.

The HRToF-CIMS was operated to switch between a negative and positive ionization mode using iodide ion water clusters $I^-\bullet(H_2O)_n$ (generated from CH_3I) and water cluster ions $H_3O^+\bullet(H_2O)_n$, respectively. The iodide ion chemistry enables measurements of HCl, Cl_2, $ClNO_2$ (Mielke et al., 2011; Osthoff et al., 2008), as well as organic and inorganic acids. Water cluster chemical ionization was discussed above; most of the results presented in this report focus on data from this mode. The sensitivity of the HRToF-CIMS can differ for each species, so individual species need to be calibrated for before quantitative data can be presented and interpreted.

For this report we present uncalibrated, qualitative data; detailed post-calibration of the instrument for species observed during DISCOVER-AQ will be done in future work.
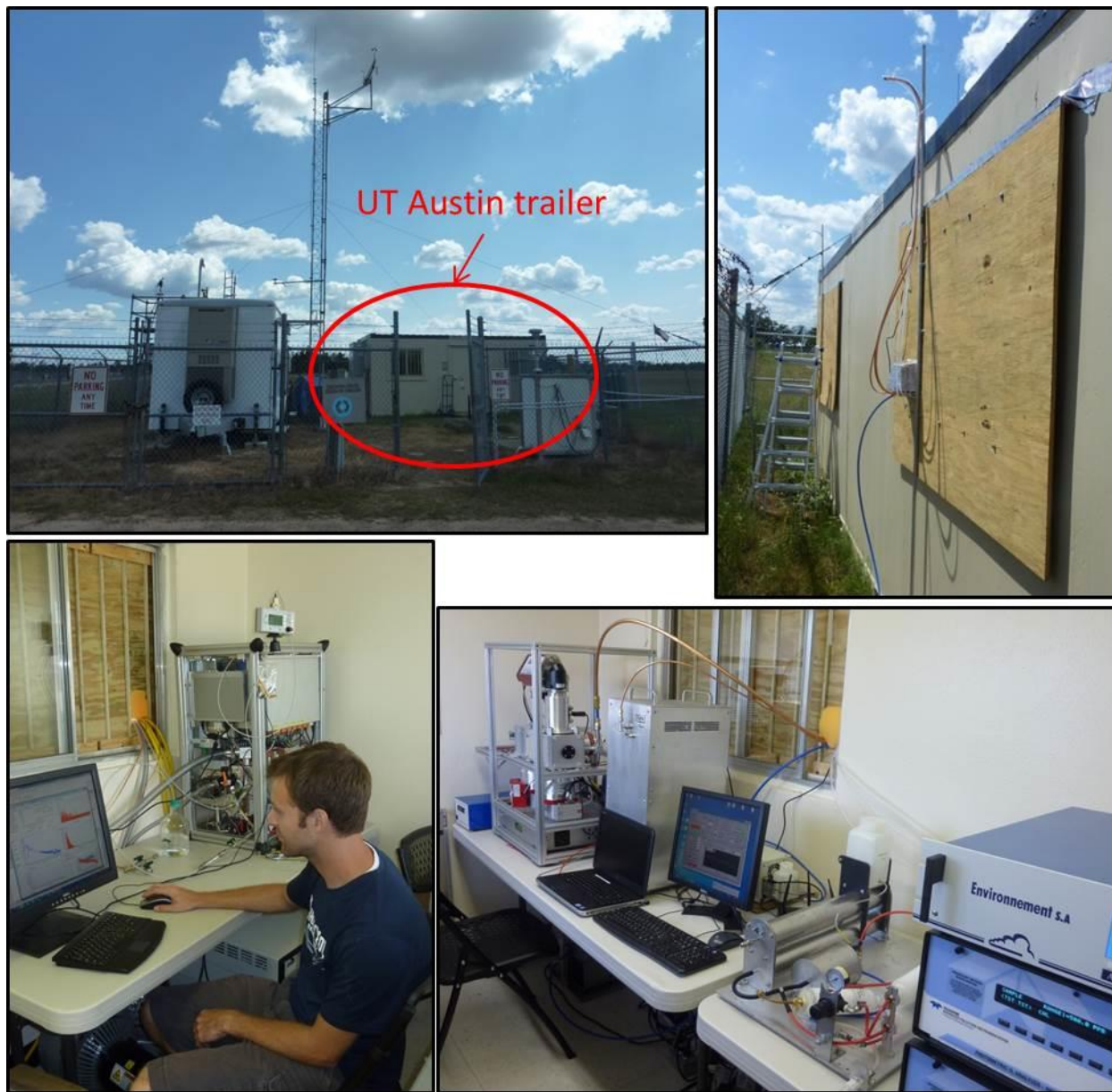
Figure 4-1. Photographs of set-up in the field showing an overview of the field site (top left), sampling lines on the outside of the trailer (top right), set-up of the HR-ToF-CIMS (bottom left) and set-up of all other instrumentation (bottom right).

4.1.1. Aerosol Chemical Speciation Monitor (ACSM) data analysis

The averaging time of the ACMS (one filter-sample cycle) was set at 2.5 min, and data were further averaged to 30 min intervals in post-analysis. The vaporizer temperature was set at the standard 600°C to ensure fast and complete vaporization of ammonium sulfate. The ACSM measures only non-refractory (NR) PM_1, i.e. compounds that flash-vaporize at 600°C. It does not measure refractory material such as black carbon, sea salt and silica (dust). Measurements of refractory aerosol components can be provided by analysis of filter samples which were collected at Conroe during DISCOVER-AQ.

We estimated the ACSM collection efficiency (CE) for these data by comparing total mass measured by the ACSM to total particle mass measured by the SEMS, which necessitates assuming a particle density. For these preliminary results we assume a standard CE of 0.5. While this CE results in decent agreement between ACSM and SEMS measurements, there are several periods over the course of the campaign when CE-corrected ACSM concentrations are lower than SEMS concentrations. These periods will be explored in more detail in further analysis. Contributions of refractory material such as black carbon, which would be detected by the SEMS but not by the ACSM, is one potential explanation for this observation.

The ACSM provides two separate measures of the NR-PM_1 that are used in this analysis: the bulk chemical composition of the particles and the total mass spectrum from which the organic mass spectrum is derived. We analyzed the data using the standard fragmentation table and batch table (Allan et al., 2004b), with a few modifications explained below. The fragmentation table attributes mass at different mass-to-charge (m/z) ratios to the different bulk species (organics, sulfate, ammonium and nitrate); the batch table specifies the ionization efficiency of the bulk species relative to nitrate.

The relative organic spectra are the contributions of the organic fragments at each m/z to the total organic mass. We report the relative importance of these fragments as f_{43}, f_{44} and f_{57}, respectively, defined as the ratio of the mass at a particular m/z to total organic mass. The mass fragments at m/z 44 mostly correspond to the CO_2^+ ion (Aiken et al., 2008) and can therefore be used as a semi-empirical measure of the extent of oxidation of the organic PM. In addition to the fragments at m/z 44, we will also focus on the fragments at m/z 43 and m/z 57. In ambient air, the fragments at m/z 43 are often primarily $C_2H_3O^+$ with a smaller contribution from $C_3H_7^+$. In ambient studies close to sources, the fragments at m/z 57 are often primarily $C_4H_9^+$ with a smaller contribution from singly-oxidized species such as $C_3H_5O^+$. Hence, f_{44} is often used as a proxy for highly oxidized OA, f_{43} is often used as a proxy for moderately oxidized OA, and f_{57} is used as a proxy for fresh, hydrocarbon-like organic aerosol (Aiken et al., 2009; Zhang et al., 2005).

Relative Ionization Efficiency (RIE)

The relative ionization efficiency (RIE) of ammonium and sulfate was measured four times over the course of the campaign, and the average values of RIE_NH4 = 5.15 and RIE_SO4 = 0.7 were used for the analysis of these data. These are typical observed values for this instrument.

Adjustments to standard fragmentation table

The fragmentation patterns of air, water and organics were evaluated using the filter measurements which are taken throughout the campaign. For air, the fragmentation pattern at m/z 44 (CO_2^+), m/z 29 ($N^{15}N^+$) and m/z 16 (O^+) was measured and adjusted, as is customary. Even though average ratios are reported here, time-dependent ratios were applied as correction to the data. $N^{15}N^+$ and CO_2^+ were calculated as fractions of the N_2^+ signal at m/z 28. The average fraction of $N^{15}N^+/N_2^+$ was 0.00730, slightly different from the standard value of 0.00736. The average ratio of CO_2^+/N_2^+ was 0.001397, different from the standard value of 0.000734. The ratio m/z 44: m/z 28 is not simply the CO_2 mixing ratio in the air but also accounts for ion transmission differences, the relative ionization efficiency of CO_2, and a correction for the m/z 14 fragmentation of nitrogen. Therefore, a coefficient deviating from the standard coefficient does not necessarily imply a difference in the CO_2 mixing ratio but may be due to differences in the other factors, which can vary between instruments. O^+ was calculated as a constant fraction of N^+. The average ratio was 0.559, different from the standard value of 0.353.

The water fragmentation pattern at m/z 16 (O^+), m/z 17 (OH^+) and m/z 18 (H_2O^+) was determined by calculating the ratios of m/z 16 and m/z 17 versus m/z 18. It was found that on average O^+ = 26.0% of H_2O^+; quite different from the 4% used in the standard fragmentation table. Furthermore, OH^+ = 26.1 % of H_2O^+, slightly different from the 25% in the standard fragmentation table). In addition to the water fragmentation, the ratio of water H_2O^+ to N_2^+ was also determined, which depends on ambient humidity. The average ratio was found to be 14%, quite different from the ratio of 1% used in the standard fragmentation table. This is not surprising considering rather humid conditions during this measurement campaign. As expected, the H_2O^+/N_2^+ exhibited a diurnal cycle similar to the measured relative humidity, which was lowest in the afternoon when temperatures were highest.

For the organic fragmentation pattern we used the recommendation by Aiken et al. (2008) that m/z 28 = 100% × m/z 44; in the original AMS fragmentation table this was set to 0%. However, differently from the recommendation of Aiken et al. (2008) we retained the ratio of m/z 18 to m/z 44 as 100%; the new recommendation was to set this ratio to 22.5%. The reason we change this was because recent work has shown that a m/z 18 / m/z 44 ratio of 100% is more

consistent with data and with calibration experiments (M. Canagaratna personal communication).

Measurements of PM nitrate

Measurements of "nitrate" (NO^+ and NO_2^+) from the ACSM can exhibit contributions from inorganic nitrate (ammonium nitrate) and organic nitrate. These different sources of nitrate have different fragmentation patters in the ACSM (NO^+ / $NO2^+$ ratios) and can therefore be separated. Specifically, in calibration experiments with ammonium nitrate the ACSM exhibited a NO^+ / NO_2^+ ratio of 3. In contrast, the laboratory experiments presented in section 3 showed much higher NO^+ / NO_2^+ ratios, with an average ratio of 8. This observation is typical for Aerodyne Aerosol Mass Spectrometers, which are similar to the ACSM (Farmer et al., 2010): while different NO^+ / NO_2^+ ratios have been found for organic nitrate formed from different VOC precursors, and for nitrates measured by different instruments, the ratio is much higher for organic nitrates than for inorganic ammonium nitrate (Farmer et al., 2010). In these field data we found the NO^+ / NO_2^+ ratio to be 10 (Figure 4-2). This suggests that, to the best of our knowledge, the particulate "nitrate" measured by the ACSM is due to organic nitrogen compounds.
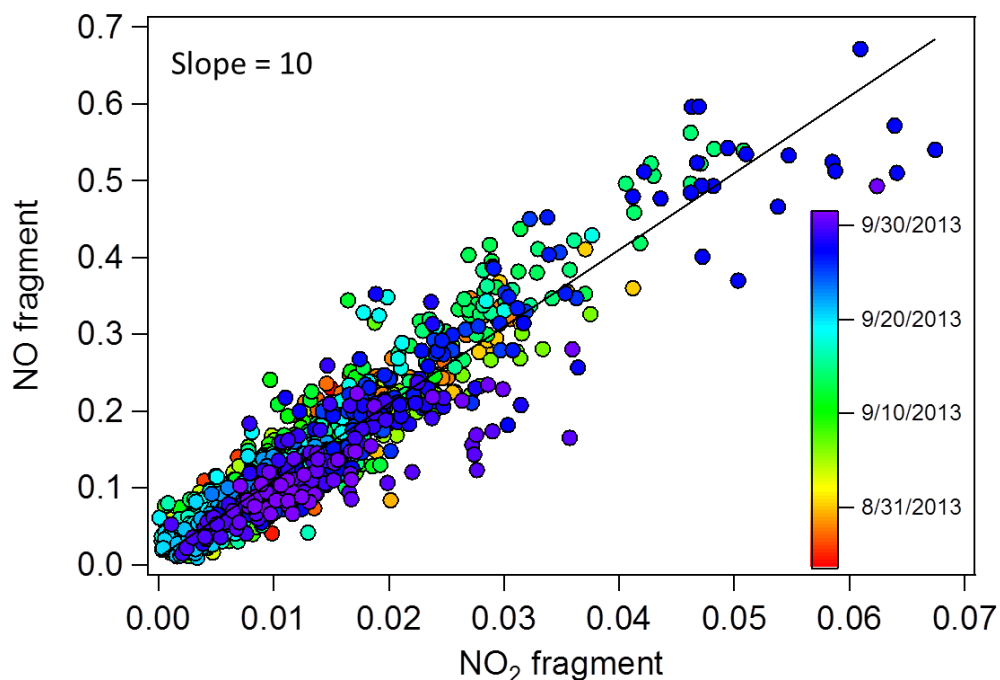
Figure 4-2. The fragmentation (NO vs. NO$_2$ fragment) of PM-Nitrate throughout the campaign. The NO/NO$_2$ ratio of 10 suggests that the measured PM-Nitrate was due to organic nitrate.

4.2 Ambient Data

4.2.1 Particle-phase composition

Figure 4-3 shows and overview of non-refractory PM_1 measured by the ACSM throughout the campaign. The NR-PM_1 was primarily composed of organics, with smaller contributions from organic nitrates and sulfate. The sulfate was presumably due to ammonium sulfate; however, further quality control of the particulate ammonium data is needed before these data can be presented. The high fraction of PM_1 due to organics (~ 70% on average) suggests that future control strategies for fine PM in Houston will need to address the formation and sources of organic PM.
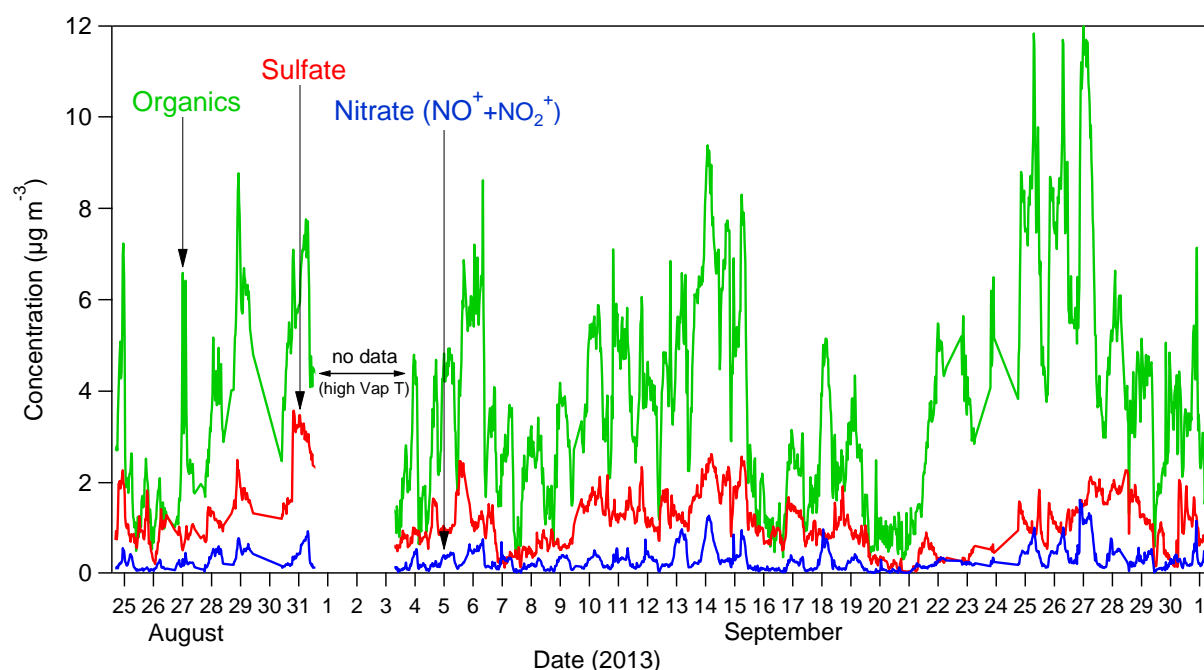
Figure 4-3. Time series of PM_1 organic, sulfate, and organic nitrate over the course of the campaign.

Figure 4-4 below shows the diurnal cycle of PM_1 organics, nitrate and sulfate throughout the campaign, as well as total $PM_{2.5}$ concentrations measured by the TCEQ. Nitrate and organics exhibited clear diurnal cycles with lower concentrations in the afternoon; the diurnal cycle of nitrate was most pronounced. Sulfate did not exhibit a diurnal cycle. The diurnal cycles of organics and nitrate (higher concentrations at night) are also consistent with total $PM_{2.5}$ concentrations measured by the TCEQ in Conroe.

Considering that the ambient relative humidity was lowest during the afternoon, the lower concentrations of PM_1 nitrate are probably not caused by hydrolysis of organic nitrates. The lack of a diurnal cycle in the PM sulfate concentrations suggests that changes in the boundary

layer height, which should affect all PM species similarly, are likely not the cause of the diurnal cycle in PM_1 organics and nitrate. The low afternoon concentrations could be caused by photolysis of organic nitrogen (ON) compounds in the afternoon. Alternatively, it is plausible that the ONs are primarily formed by night-time chemistry with the nitrate radical, resulting in higher concentrations at night than during the day. Potential effects of night-time and nitrate-radical chemistry on air-quality in Conroe will be investigated in more detail in future work.
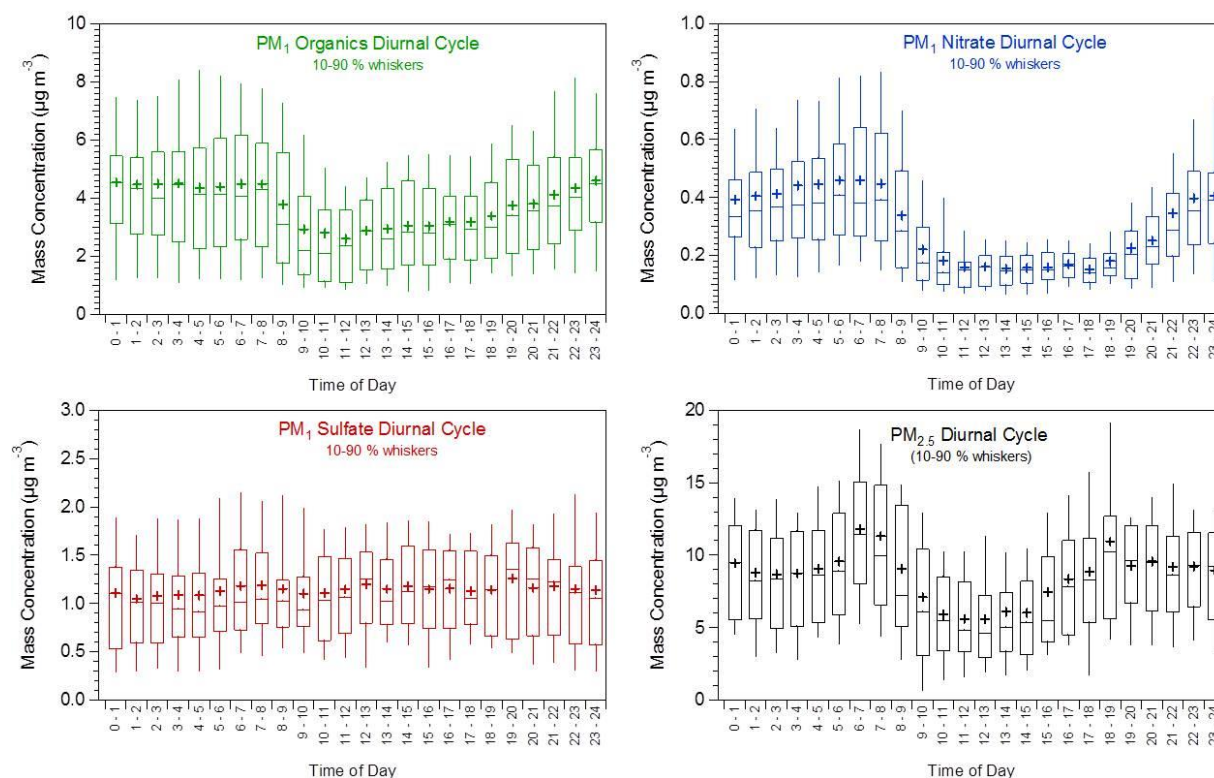
Figure 4-4. Diurnal cycle of organics (top left), nitrate (top right) and sulfate (bottom left) from the UT-Austin ACSM, and diurnal cycle of total $PM_{2.5}$ measured by the TCEQ using a tapered element oscillating microbalance (TEOM) monitor (uncorrected data).

As mentioned in section 4.1.1 above, the fraction of the total organic signal due to molecular fragments at m/z 43 and m/z 44 (f_{43} and f_{44}, respectively) can be used as a measure of the extent of oxidation of the organic particulate matter. More specifically, fragments at m/z 43 are used as a proxy for moderately oxidized organic aerosol and fragments and m/z 44 are used as a proxy for highly oxidized organic aerosol. Figure 4-5 shows the diurnal cycle of f_{44} and f_{43}, showing that f_{44} increases in the afternoon as f_{43} decreases, consistent with singly oxidized species being transformed to doubly oxidized species. These are signs of the photochemical processing of organic aerosol components in the Houston region. Further analysis of the particle-phase data collected in Conroe will shed more light on the photochemical processing of pollutants.
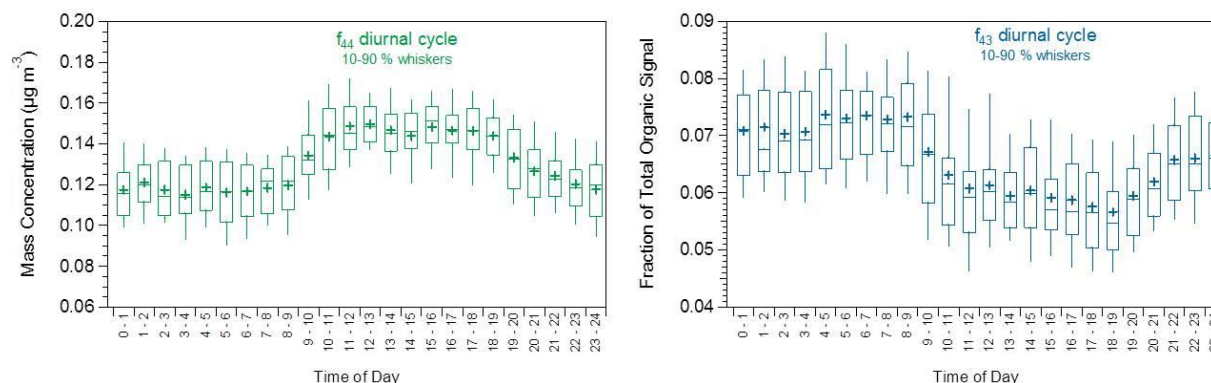
Figure 4-5. Diurnal cycle of f_{44} (left) and f_{43} (right) showing the photochemical transformation of organic PM during the day.

4.2.2 Gas-phase organic nitrates and likely VOC precursors

Preliminary analysis of the gas-phase data collected during DISCOVER-AQ suggests that many organic nitrogen species were present and observed during the campaign. Overall, over 100 organic nitrogen species were identified in positive ionization mode alone, and they exhibited different diurnal variation. Calibration of the instrument and quantification for these organic nitrogen compounds is part of ongoing work. Figure 4-6 below shows a representative diurnal cycle of one organic nitrogen compound, $C_9H_{15}NO_4$, which could be formed from the photo-oxidation of alpha-pinene. Further analysis of the trends of these species – with time of day (diurnal cycle), wind direction and other meteorological conditions – will be performed in future work.

Data from the HR-ToF-CIMS collected during DISCOVER-AQ also provide insights into potential VOC precursors of oxidized organics, organic nitrogen compounds and particulate matter. Figure 4-7 below shows the time series of isoprene throughout the campaign. Instrument calibration and further analysis of the observed trend in the concentrations of isoprene will be done in future work.
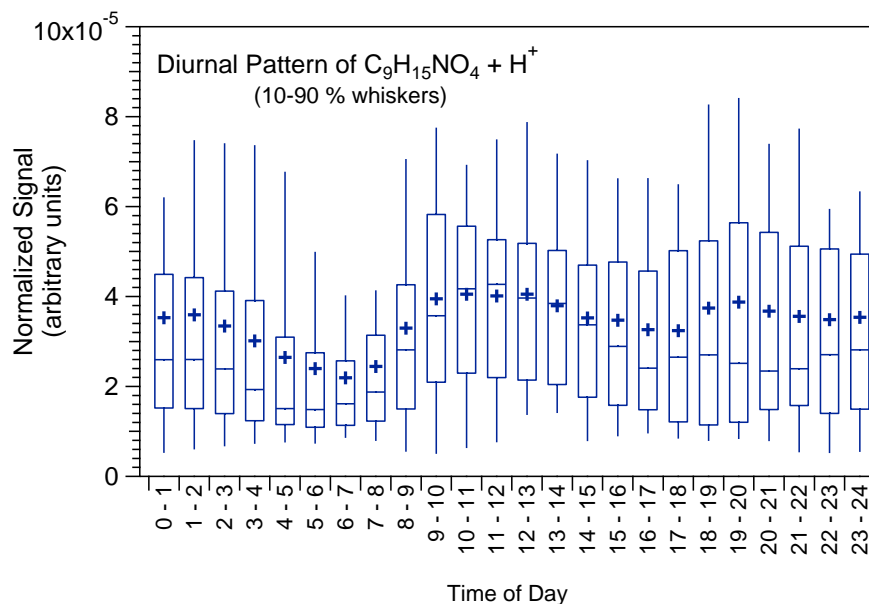
Figure 4-6. Diurnal cycle of $C_9H_{15}NO_4$ observed during DISCOVER-AQ. Quantification of gas-phase species and further investigation of their sources and variation are part of future work.
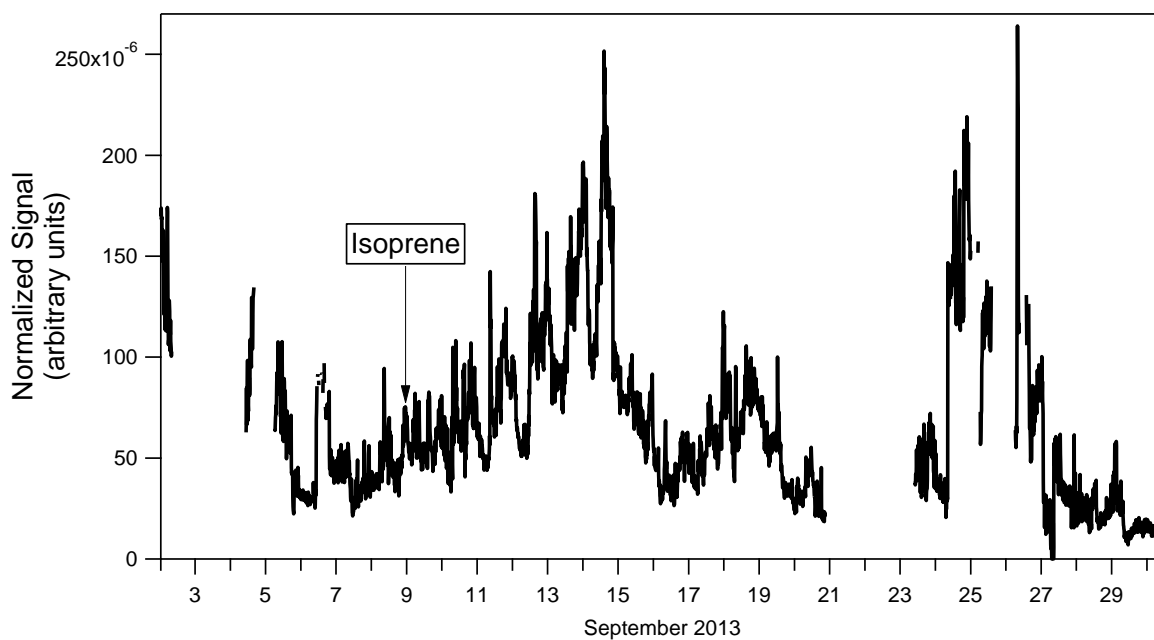
Figure 4-7. Time series of isoprene observed during DISCOVER-AQ.

4.2.3 Discussion of ambient data and future analysis

Measurements of gas- and particle phase composition and concentrations were performed in Conroe, TX, during the DISCOVER-AQ campaign. Preliminary analysis of the data suggests that a large fraction of fine PM was due to organic material, that photochemical transformation of pollutants was observed in the gas- and particle-phases, and that significant concentrations of organic nitrogen compounds were observed in the gas- and particle-phases. Additional analysis and quality assurance of the data will be done as part of future work.

5.0 Conclusions and Recommendations

Photochemical modeling, environmental chamber experiments and ambient measurements were combined to explore the formation of organic nitrogen species (ONs), their interaction with organic aerosol (OA) and their overall effect on the production of ozone. Environmental chamber experiments found that significant concentrations of ON formed from all precursors investigated and that the ONs reversibly partition between the gas- and particle-phases. Ambient observations found that ONs are also abundant near Houston, TX in the gas- and particle phases. The Carbon Bond mechanism was updated, and in the newest version (CB6r2) organic nitrates are divided into simple alkyl nitrates that remain in the gas-phase and multi-functional ONs that can partition into OA. The uptake of multi-functional ONs by organic aerosol (OA) and their hydrolysis in the particle phase were added to the Comprehensive Air quality Model with extensions (CAMx). Regional modeling simulations using CAMx with CB6r2 showed improved performance in simulating ozone and in simulating the partitioning of NO_y between ONs and nitric acid.

Uncertainty in the atmospheric fate of ONs adds substantial uncertainty in modeling regional O3 and other oxidants. Additional laboratory studies and ambient measurements are needed to better quantify partitioning of ONs to aerosol, forming ANs, and the subsequent chemical fate of ANs. We make the following recommendations for additional environmental chamber experiments and other activities to support improvements in the representation of organic nitrates in chemical transport models:

1. Environmental chamber experiments forming ONs from different precursors and at different relative humidity to quantify the hydrolysis rate of ONs. (The lifetime of 6 hours currently used in CB6r2 is based on limited experimental and ambient data.)

2. Analysis of experimental data to calculate the gas-particle partitioning coefficient of ONs (the gas-particle partitioning currently used in CB6r2 is based on a single peer-reviewed publication). This analysis necessitates quantification of ONs in the gas-phase and the particle-phase, or quantification of total ON formation and the amount of ONs in the gas-phase or particle-phase.

A more systematic analysis of the gas-particle partitioning of ONs with varying environmental chamber temperature would support this analysis.

3. Analysis of ambient data to calculate the gas-particle partitioning factor of organic nitrates. This analysis would necessitate quantification of ONs in the gas-phase and the particle phase.

The ON scheme implemented in CB6r2 is simple and generally consistent with available studies and improves the performance of CB6r2 in simulating regional O_3 and NOy speciation compared to CB6r1. CB6r2 is recommended over preceding versions of CB6 and CB05.

6.0 References

Aiken, A. C., DeCarlo, P. F., Kroll, J. H., Worsnop, D. R., Huffman, J. A., Docherty, K., Ulbrich, I. M., Mohr, C., Kimmel, J. R., Sueper, D., Sun, Y., Zhang, Q., Trimborn, A. M., Northway, M. J., Ziemann, P. J., Canagaratna, M. R., Alfarra, M. R., Prevot, A. S. H., Dommen, J., Duplissy, J., Metzger, A., Baltensperger, U. and Jimenez, J. L.: O/C and OM/OC Ratios of Primary, Secondary, and Ambient Organic Aerosols with High Resolution Time-of-Flight Aerosol Mass Spectrometry, Environ. Sci. Technol., 42, 4478–4485, 2008.

Aiken, A. C., Salcedo, D., Cubison, M. J., Huffman, J. A., DeCarlo, P. F., Ulbrich, I. M., Docherty, K. S., Sueper, D., Kimmel, J. R., Worsnop, D. R., Trimborn, A., Northway, M., Stone, E. A., Schauer, J. J., Volkamer, R. M., Fortner, E., de Foy, B., Wang, J., Laskin, A., Shutthanandan, V., Zheng, J., Zhang, R., Gaffney, J., Marley, N. A., Paredes-Miranda, G., Arnott, W. P., Molina, L. T., Sosa, G. and Jimenez, J. L.: Mexico City aerosol analysis during MILAGRO using high resolution aerosol mass spectrometry at the urban supersite (T0) - Part 1: Fine particle composition and organic source apportionment, Atmos. Chem. Phys., 9, 6633–6653, 2009.

Allan, J. D., Delia, A. E., Coe, H., Bower, K. N., Alfarra, M. R., Jimenez, J. L., Middlebrook, A. M., Drewnick, F., Onasch, T. B., Canagaratna, M. R., Jayne, J. T. and Worsnop, D. R.: A generalised method for the extraction of chemically resolved mass spectra from Aerodyne aerosol mass spectrometer data, J. Aerosol Sci., 35(7), 909–922, doi:10.1016/j.jaerosci.2004.02.007, 2004a.

Allan, J. D., Delia, A. E., Coe, H., Bower, K. N., Alfarra, M. R., Jimenez, J. L., Middlebrook, A. M., Drewnick, F., Onasch, T. B., Canagaratna, M. R., Jayne, J. T. and Worsnop, D. R.: A generalised method for the extraction of chemically resolved mass spectra from aerodyne aerosol mass spectrometer data, J. Aerosol Sci., 35(7), 909–922 [online] Available from: <Go to ISI>://000222832800008, 2004b.

Aschmann, S. M., Tuazon, E. C., Arey, J. and Atkinson, R.: Products of the OH radical-initiated reactions of 2-propyl nitrate, 3-methyl-2-butyl nitrate and 3-methyl-2-pentyl nitrate, Atmos. Environ., 45(9), 1695–1701, doi:10.1016/j.atmosenv.2010.12.061, 2011.

Bertram, T. H., Kimmel, J. R., Crisp, T. a., Ryder, O. S., Yatavelli, R. L. N., Thornton, J. a., Cubison, M. J., Gonin, M. and Worsnop, D. R.: A field-deployable, chemical ionization time-of-flight mass spectrometer, Atmos. Meas. Tech., 4(7), 1471–1479, doi:10.5194/amt-4-1471-2011, 2011.

Browne, E. C., Min, K.-E., Wooldridge, P. J., Apel, E., Blake, D. R., Brune, W. H., Cantrell, C. a., Cubison, M. J., Diskin, G. S., Jimenez, J. L., Weinheimer, a. J., Wennberg, P. O., Wisthaler, a. and Cohen, R. C.: Observations of total $RONO_2$ over the boreal forest: NO_x sinks and HNO_3 sources, Atmos. Chem. Phys., 13(9), 4543–4562, doi:10.5194/acp-13-4543-2013, 2013.

Day, D. a., Liu, S., Russell, L. M. and Ziemann, P. J.: Organonitrate group concentrations in submicron particles with high nitrate and organic fractions in coastal southern California, Atmos. Environ., 44(16), 1970–1979, doi:10.1016/j.atmosenv.2010.02.045, 2010.

Dudhia, J., The WRF Model: 2012 Annual Update. Presented at the 13th Annual WRF Users' Workshop, 25-29 June 2012, Boulder, CO (http://www.mmm.ucar.edu/wrf/users/workshops/WS2012/ppts/1.1.pdf), 2012

EPA. Air Quality Modeling Final Rule Technical Support Document. Office of Air Quality Planning and Standards, Air Quality Assessment Division, U.S. Environmental Protection Agency, Research Triangle Park, NC (http://www.epa.gov/crossstaterule/pdfs/AQModeling.pdf), 2011

Farmer, D. K., Matsunaga, a, Docherty, K. S., Surratt, J. D., Seinfeld, J. H., Ziemann, P. J. and Jimenez, J. L.: Response of an aerosol mass spectrometer to organonitrates and organosulfates and implications for atmospheric chemistry., Proc. Natl. Acad. Sci. U. S. A., 107(15), 6670–5, doi:10.1073/pnas.0912340107, 2010.

Guenther, A. B., Jiang, X., Heald, C.L. Sakulyanontvittaya, T., Duhl, T., Emmons, L. K. and Wang, X.: The Model of Emissions of Gases and Aerosols from Nature version 2.1 (MEGAN2.1): an extended and updated framework for modeling biogenic emissions. , 5, 1503-1560., Geosci. Model Dev. Discuss., 5, 1503–1560, 2012.

Hildebrandt, L., Donahue, N. M. and Pandis, S. N.: High formation of secondary organic aerosol from the photo-oxidation of toluene, Atmos. Chem. Phys., (9), 2973–2986, 2009.

Horowitz, L. W., Fiore, A. M., Milly, G. P., Cohen, R. C., Perring, A. E., Wooldridge, P. J., Hess, P. G., Emmons, L. K. and Lamarque, J.: Observational constraints on the chemistry of isoprene nitrates over the eastern United States, J. Geophys. Res., 112(12), doi:10.1029/2006JD007747, 2007.

Kames, J. and Schurath, U.: Alkyl Nitrates and Bifunctional Nitrates of Atmospheric Interest : Henry's Law Constants and Their Temperature Dependencies, J. Atmos. Chem., 15, 79–95, 1992.

Kebabian, P. L., Wood, E. C., Herdon, S. C. and Freedman, A.: A Practical Alternative to Chemiluminescence-Based Detection of Nitrogen Dioxide: Cavity Attenuated Phase Shift Spectroscopy, Environ. Sci. Technol., 42, 6040–6045, 2008.

Kemball-Cook, S., J. Johnson and G. Yarwood, Continuation on Use of Satellite Nitrogen Dioxide (NO_2) Data, Final Report for TCEQ project 582-11-10365-FY13-10, August 2013.

Liu, S., Shilling, J. E., Song, C., Hiranuma, N., Zaveri, R. a. and Russell, L. M.: Hydrolysis of Organonitrate Functional Groups in Aerosol Particles, Aerosol Sci. Technol., 46(12), 1359–1369, doi:10.1080/02786826.2012.716175, 2012.

Matsunaga, A., Docherty, K. S., Lim, Y. B. and Ziemann, P. J.: Composition and yields of secondary organic aerosol formed from OH radical-initiated reactions of linear alkenes in the presence of NOx: Modeling and measurements, Atmos. Environ., 43(6), 1349–1357, doi:10.1016/j.atmosenv.2008.12.004, 2009.

Mielke, L. H., Furgeson, A. and Osthoff, H. D.: Observation of $ClNO_2$ in a mid-continental urban environment., Environ. Sci. Technol., 45(20), 8889–96, doi:10.1021/es201955u, 2011.

Odum, J. R., Hoffmann, T., Bowman, F., Collins, D., Flagan, R. C. and Seinfeld, J. H.: Gas/particle partitioning and secondary organic aerosol yields, Environ. Sci. Technol., 30(8), 2580–2585 [online] Available from: <Go to ISI>://A1996VA63700047, 1996.

Osthoff, H. D., Roberts, J. M., Ravishankara, A. R., Williams, E. J., Lerner, B. M., Sommariva, R., Bates, T. S., Coffman, D., Quinn, P. K., Dibb, J. E., Stark, H., Burkholder, J. B., Talukdar, R. K., Meagher, J., Fehsenfeld, F. C. and Brown, S. S.: High levels of nitryl chloride in the polluted subtropical marine boundary layer, Nat. Geosci., 1(5), 324–328, doi:10.1038/ngeo177, 2008.

Pankow, J. F.: An absorption model of the gas/aerosol partitioning involved in the formation of secondary organic aerosol., Atmos. Environ., 28(2), 189–193 [online] Available from: <Go to ISI>://A1994NR21200003, 1994.

Paulot, F., Crounse, J. D., Kjaergaard, H. G., Kroll, J. H., Seinfeld, J. H. and Wennberg, P. O.: Isoprene photooxidation : new insights into the production of acids and organic nitrates, Atmos. Chem. Phys., 9, 1479–1501, 2009.

Perraud, V., Bruns, E. A., Ezell, M. J., Johnson, S. N., Yong, Y., Alexander, M. L., Zelenyuk, A., Imre, D., Chang, W. L., Dabdub, D., Pankow, J. F. and Finlayson-Pitts, B. J.: Nonequilibrium atmospheric secondary organic aerosol formation and growth, Proc. Natl. Acad. Sci., 109(8), 2836–2841, doi:10.1073/pnas.1119909109, 2012.

Perring, a E., Pusede, S. E. and Cohen, R. C.: An Observational Perspective on the Atmospheric Impacts of Alkyl and Multifunctional Nitrates on Ozone and Secondary Organic Aerosol., Chem. Rev., doi:10.1021/cr300520x, 2013.

Perring, a. E., Bertram, T. H., Wooldridge, P. J., Fried, a., Heikes, B. G., Dibb, J., Crounse, J. D., Wennberg, P. O., Blake, N. J., Blake, D. R., Brune, W. H., Singh, H. B. and Cohen, R. C.: Airborne observations of total $RONO_2$: new constraints on the yield and lifetime of isoprene nitrates, Atmos. Chem. Phys., 9(4), 1451–1463, doi:10.5194/acp-9-1451-2009, 2009.

Roberts, J. M.: CHEMISTRY OF ORGANIC NITRATES, Atmos. Environ., 24(2), 243–287, 1990.

Rollins, a. W., Pusede, S., Wooldridge, P., Min, K.-E., Gentner, D. R., Goldstein, a. H., Liu, S., Day, D. a., Russell, L. M., Rubitschun, C. L., Surratt, J. D. and Cohen, R. C.: Gas/particle partitioning of total alkyl nitrates observed with TD-LIF in Bakersfield, J. Geophys. Res. Atmos., 118(12), 6651–6662, doi:10.1002/jgrd.50522, 2013.

Saylor, R. D. and Stein, A. F.: Identifying the causes of differences in ozone production from the CB05 and CBMIV chemical mechanisms, Geosci. Model Dev., 5, 257–268, 2012.

Seinfeld, J. H. and Pandis, S. N.: Atmospheric Chemistry and Physics, Second Edi., John Wiley & Sons, Hoboken., 2006.

Shepson, P. B., Mackay, E. and Muthuramu, K.: Henry ' s Law Constants and Removal Processes for Several Atmospheric -Hydroxy Alkyl Nitrates, Environ. Sci. Technol., 30(12), 3618–3623, 1996.

Shepson, P. B. In Volatile Organic Compounds in the Atmosphere, Koppmann, R., Ed., Blackwell Publishing: Oxford, 2007.

Singh, H. B., Brune, W. H., Crawford, J. H., Jacob, D. J. and Russell, P. B.: Overview of the summer 2004 Intercontinental Chemical Transport Experiment–North America (INTEX-A), J. Geophys. Res., 111(D24), D24S01, doi:10.1029/2006JD007905, 2006.

Singh, H. B., Salas, L., Herlth, D., Kolyer, R., Czech, E., Avery, M., Crawford, J. H., Pierce, R. B., Sachse, G. W., Blake, D. R., Cohen, R. C., Bertram, T. H., Perring, a., Wooldridge, P. J., Dibb, J., Huey, G., Hudman, R. C., Turquety, S., Emmons, L. K., Flocke, F., Tang, Y., Carmichael, G. R. and Horowitz, L. W.: Reactive nitrogen distribution and partitioning in the North American troposphere and lowermost stratosphere, J. Geophys. Res., 112(D12), D12S04, doi:10.1029/2006JD007664, 2007.

Yarwood, G., Rao, S., Yocke, M., Whitten, G.Z. Updates to the Carbon Bond chemical mechanism: CB05. Final Report prepared for U.S. Environmental Protection Agency. (http://www.camx.com/publ/pdfs/CB05_Final_Report_120805.pdf), 2005.

Yarwood, G., Heo, G., Carter, W. P. L. and Whitten, G. Z.: Environmental Chamber Experiments to Evaluate NOx Sinks and Recycling in Atmospheric Chemical Mechanisms, Environ, Novato., 2012.

Yatavelli, R. L. N., Lopez-Hilfiker, F., Wargo, J. D., Kimmel, J. R., Cubison, M. J., Bertram, T. H., Jimenez, J. L., Gonin, M., Worsnop, D. R. and Thornton, J. a.: A Chemical Ionization High-Resolution Time-of-Flight Mass Spectrometer Coupled to a Micro Orifice Volatilization Impactor (MOVI-HRToF-CIMS) for Analysis of Gas and Particle-Phase Organic Species, Aerosol Sci. Technol., 46(12), 1313–1327, doi:10.1080/02786826.2012.712236, 2012.

Zhang, Q., Alfarra, M. R., Worsnop, D. R., Allan, J. D., Coe, H., Canagaratna, M. R. and Jimenez, J. L.: Deconvolution and quantification of hydrocarbon-like and oxygenated organic aerosols based on aerosol mass spectrometry, Environ. Sci. Technol., 39(13), 4938–4952, 2005.

Appendix A

Rxn	Reactants = Products	Rate Parameters				
		k(298)	A	Ea	B	notes
1	NO2 = NO + O	Photolysis				a
2	O + O2 + M = O3 + M	5.78E-34	5.68E-34	0.0	-2.60	a
3	O3 + NO = NO2	1.73E-14	1.40E-12	1310.0	0.00	a
4	O + NO + M = NO2 + M	1.01E-31	1.00E-31	0.0	-1.60	a
5	O + NO2 = NO	1.03E-11	5.50E-12	-188.0	0.00	a
6	O + NO2 = NO3	2.11E-12	Falloff, F=0.60 ,N=1.00			a
		k_0	1.30E-31	0.0	-1.50	
		k_∞	2.30E-11	0.0	0.24	
7	O + O3 =	7.96E-15	8.00E-12	2060.0	0.00	a
8	O3 = O	Photolysis				a
9	O3 = O1D	Photolysis				a
10	O1D + M = O + M	3.28E-11	2.23E-11	-115.0	0.00	a
11	O1D + H2O = 2 OH	2.14E-10	2.14E-10			a
12	O3 + OH = HO2	7.25E-14	1.70E-12	940.0	0.00	a
13	O3 + HO2 = OH	2.01E-15	2.03E-16	-693.0	4.57	a
14	OH + O = HO2	3.47E-11	2.40E-11	-110.0	0.00	a
15	HO2 + O = OH	5.73E-11	2.70E-11	-224.0	0.00	a
16	OH + OH = O	1.48E-12	6.20E-14	-945.0	2.60	a
17	OH + OH = H2O2	5.25E-12	Falloff, F=0.50 ,N=1.13			a
		k_0	6.90E-31	0.0	-0.80	
		k_∞	2.60E-11	0.0	0.00	
18	OH + HO2 =	1.11E-10	4.80E-11	-250.0	0.00	a
19	HO2 + HO2 = H2O2	2.90E-12	k = k1 + k2[M]			a
		k1	2.20E-13	-600.0	0.00	
		k2	1.90E-33	-980.0	0.00	
20	HO2 + HO2 + H2O = H2O2	6.53E-30	k = k1 + k2[M]			a
		k1	3.08E-34	-2800.0	0.00	
		k2	2.66E-54	-3180.0	0.00	
21	H2O2 = 2 OH	Photolysis				a
22	H2O2 + OH = HO2	1.70E-12	2.90E-12	160.0	0.00	a
23	H2O2 + O = OH + HO2	1.70E-15	1.40E-12	2000.0	0.00	a
24	NO + NO + O2 = 2 NO2	1.95E-38	3.30E-39	-530.0	0.00	a
25	HO2 + NO = OH + NO2	8.54E-12	3.45E-12	-270.0	0.00	a
26	NO2 + O3 = NO3	3.52E-17	1.40E-13	2470.0	0.00	a
27	NO3 = NO2 + O	Photolysis				b
28	NO3 = NO	Photolysis				b
29	NO3 + NO = 2 NO2	2.60E-11	1.80E-11	-110.0	0.00	a
30	NO3 + NO2 = NO + NO2	6.56E-16	4.50E-14	1260.0	0.00	b
31	NO3 + O = NO2	1.70E-11	1.70E-11			a
32	NO3 + OH = HO2 + NO2	2.00E-11	2.00E-11			a
33	NO3 + HO2 = OH + NO2	4.00E-12	4.00E-12			a
34	NO3 + O3 = NO2	1.00E-17	1.00E-17			k
35	NO3 + NO3 = 2 NO2	2.28E-16	8.50E-13	2450.0	0.00	b
36	NO3 + NO2 = N2O5	1.24E-12	Falloff, F=0.35 ,N=1.33			a
		k_0	3.60E-30	0.0	-4.10	
		k_∞	1.90E-12	0.0	0.20	

Rxn	Reactants = Products	k(298)	A	Ea	B	notes
			Rate Parameters			
37	N2O5 = NO3 + NO2	4.46E-02	Falloff, F=0.35 ,N=1.33			a
		k_0	1.30E-03	11000.0	-3.50	
		k_∞	9.70E+14	11080.0	0.10	
38	N2O5 = NO2 + NO3	Photolysis				a
39	N2O5 + H2O = 2 HNO3	1.00E-22	1.00E-22			a
40	NO + OH = HONO	9.77E-12	Falloff, F=0.81 ,N=0.87			a
		k_0	7.40E-31	0.0	-2.40	
		k_∞	3.30E-11	0.0	-0.30	
41	NO + NO2 + H2O = 2 HONO	5.00E-40	5.00E-40			c
42	HONO + HONO = NO + NO2	1.00E-20	1.00E-20			c,m
43	HONO = NO + OH	Photolysis				a
44	HONO + OH = NO2	5.98E-12	2.50E-12	-260.0	0.00	a
45	NO2 + OH = HNO3	1.06E-11	Falloff, F=0.60 ,N=1.00			b; v an option
		k_0	1.80E-30	0.0	-3.00	
		k_∞	2.80E-11	0.0	0.00	
46	HNO3 + OH = NO3	1.54E-13	k = k0+k3M/(1+k3M/k2)			a
		k0	2.40E-14	-460.0	0.00	
		k2	2.70E-17	-2199.0	0.00	
		k3	6.50E-34	-1335.0	0.00	
47	HNO3 = OH + NO2	Photolysis				a
48	HO2 + NO2 = PNA	1.38E-12	Falloff, F=0.60 ,N=1.00			a
		k_0	1.80E-31	0.0	-3.20	
		k_∞	4.70E-12	0.0	0.00	
49	PNA = HO2 + NO2	8.31E-02	Falloff, F=0.60 ,N=1.00			a
		k_0	4.10E-05	10650.0	0.00	
		k_∞	4.80E+15	11170.0	0.00	
50	PNA = 0.59 HO2 + 0.59 NO2 + 0.41 OH + 0.41 NO3	Photolysis				a
51	PNA + OH = NO2	3.24E-12	3.20E-13	-690.0	0.00	a
52	SO2 + OH = SULF + HO2	8.12E-13	Falloff, F=0.53 ,N=1.10			a
		k_0	4.50E-31	0.0	-3.90	
		k_∞	1.30E-12	0.0	-0.70	
53	C2O3 + NO = NO2 + MEO2 + RO2	1.98E-11	7.50E-12	-290.0	0.00	a
54	C2O3 + NO2 = PAN	9.40E-12	Falloff, F=0.30 ,N=1.41			a, l
		k_0	2.70E-28	0.0	-7.10	
		k_∞	1.20E-11	0.0	-0.90	
55	PAN = NO2 + C2O3	2.98E-04	Falloff, F=0.30 ,N=1.41			a, l
		k_0	4.90E-03	12100.0	0.00	
		k_∞	5.40E+16	13830.0	0.00	
56	PAN = 0.6 NO2 + 0.6 C2O3 + 0.4 NO3 + 0.4 MEO2 + 0.4 RO2	Photolysis				a
57	C2O3 + HO2 = 0.41 PACD + 0.15 AACD + 0.15 O3 + 0.44 MEO2 + 0.44 RO2 + 0.44 OH	1.39E-11	5.20E-13	-980.0	0.00	a
58	C2O3 + RO2 = C2O3	1.30E-11	8.90E-13	-800.0	0.00	a
59	C2O3 + C2O3 = 2 MEO2 + 2 RO2	1.55E-11	2.90E-12	-500.0	0.00	a
60	C2O3 + CXO3 = MEO2 + ALD2 + XO2H + 2 RO2	1.55E-11	2.90E-12	-500.0	0.00	a
61	CXO3 + NO = NO2 + ALD2 + XO2H + RO2	2.10E-11	6.70E-12	-340.0	0.00	a
62	CXO3 + NO2 = PANX	9.40E-12	k = kref * K			a, l
		k(ref)	ref = 54			
		K	1.00E+00	0.0	0.00	

Rxn	Reactants = Products	Rate Parameters				
		k(298)	A	Ea	B	notes
63	PANX = NO2 + CXO3	2.98E-04	k = kref * K			a, l
		k(ref)	ref = 55			
		K	1.00E+00	0.0	0.00	
64	PANX = 0.6 NO2 + 0.6 CXO3 + 0.4 NO3 + 0.4 ALD2 + 0.4 XO2H + 0.4 RO2	Photolysis				a
65	CXO3 + HO2 = 0.41 PACD + 0.15 AACD + 0.15 O3 + 0.44 ALD2 + 0.44 XO2H + 0.44 RO2 + 0.44 OH	1.39E-11	5.20E-13	-980.0	0.00	a
66	CXO3 + RO2 = 0.8 ALD2 + 0.8 XO2H + 0.8 RO2	1.30E-11	8.90E-13	-800.0	0.00	a
67	CXO3 + CXO3 = 2 ALD2 + 2 XO2H + 2 RO2	1.71E-11	3.20E-12	-500.0	0.00	a
68	RO2 + NO = NO	8.03E-12	2.40E-12	-360.0	0.00	a
69	RO2 + HO2 = HO2	7.03E-12	4.80E-13	-800.0	0.00	a
70	RO2 + RO2 =	3.48E-13	6.50E-14	-500.0	0.00	a
71	MEO2 + NO = FORM + HO2 + NO2	7.70E-12	2.30E-12	-360.0	0.00	a
72	MEO2 + HO2 = 0.9 MEPX + 0.1 FORM	5.21E-12	3.80E-13	-780.0	0.00	a
73	MEO2 + C2O3 = FORM + 0.9 HO2 + 0.9 MEO2 + 0.1 AACD + 0.9 RO2	1.07E-11	2.00E-12	-500.0	0.00	a
74	MEO2 + RO2 = 0.685 FORM + 0.315 MEOH + 0.37 HO2 + RO2	3.48E-13	k = kref * K			a
		k(ref)	ref = 70			
		K	1.00E+00	0.0	0.00	
75	XO2H + NO = NO2 + HO2	9.04E-12	2.70E-12	-360.0	0.00	a
76	XO2H + HO2 = ROOH	9.96E-12	6.80E-13	-800.0	0.00	a
77	XO2H + C2O3 = 0.8 HO2 + 0.8 MEO2 + 0.2 AACD + 0.8 RO2	1.30E-11	k = kref * K			a
		k(ref)	ref = 58			
		K	1.00E+00	0.0	0.00	
78	XO2H + RO2 = 0.6 HO2 + RO2	3.48E-13	k = kref * K			a
		k(ref)	ref = 70			
		K	1.00E+00	0.0	0.00	
79	XO2 + NO = NO2	9.04E-12	k = kref * K			a
		k(ref)	ref = 75			
		K	1.00E+00	0.0	0.00	
80	XO2 + HO2 = ROOH	9.96E-12	k = kref * K			a
		k(ref)	ref = 76			
		K	1.00E+00	0.0	0.00	
81	XO2 + C2O3 = 0.8 MEO2 + 0.2 AACD + 0.8 RO2	1.30E-11	k = kref * K			a
		k(ref)	ref = 58			
		K	1.00E+00	0.0	0.00	
82	XO2 + RO2 = RO2	3.48E-13	k = kref * K			a
		k(ref)	ref = 70			
		K	1.00E+00	0.0	0.00	
83	XO2N + NO = 0.5 NTR1 + 0.5 NTR2	9.04E-12	k = kref * K			a,w
		k(ref)	ref = 75			
		K	1.00E+00	0.0	0.00	
84	XO2N + HO2 = ROOH	9.96E-12	k = kref * K			a
		k(ref)	ref = 76			
		K	1.00E+00	0.0	0.00	
85	XO2N + C2O3 = 0.8 HO2 + 0.8 MEO2 + 0.2 AACD + 0.8 RO2	1.30E-11	k = kref * K			a
		k(ref)	ref = 58			
		K	1.00E+00	0.0	0.00	
86	XO2N + RO2 = RO2	3.48E-13	k = kref * K			a
		k(ref)	ref = 70			

Rxn	Reactants = Products	Rate Parameters				
		k(298)	A	Ea	B	notes
		K	1.00E+00	0.0	0.00	
87	MEPX + OH = 0.6 MEO2 + 0.6 RO2 + 0.4 FORM + 0.4 OH	1.00E-11	5.30E-12	-190.0	0.00	a
88	MEPX = MEO2 + RO2 + OH	Photolysis				a
89	ROOH + OH = 0.54 XO2H + 0.06 XO2N + 0.6 RO2 + 0.4 OH	6.05E-12	3.20E-12	-190.0	0.00	a
90	ROOH = HO2 + OH	Photolysis				a
91	NTR1 + OH = NTR2	2.00E-12	8.10E-13			w
92	NTR1 = NO2	Photolysis				a
93	FACD + OH = HO2	4.50E-13	4.50E-13			a
94	AACD + OH = MEO2 + RO2	6.93E-13	4.00E-14	-850.0	0.00	a
95	PACD + OH = C2O3	6.93E-13	4.00E-14	-850.0	0.00	a
96	FORM + OH = HO2 + CO	8.49E-12	5.40E-12	-135.0	0.00	a
97	FORM = 2 HO2 + CO	Photolysis				a
98	FORM = CO + H2	Photolysis				a
99	FORM + O = OH + HO2 + CO	1.58E-13	3.40E-11	1600.0	0.00	b
100	FORM + NO3 = HNO3 + HO2 + CO	5.50E-16	5.50E-16			a
101	FORM + HO2 = HCO3	7.90E-14	9.70E-15	-625.0	0.00	a
102	HCO3 = FORM + HO2	1.51E+02	2.40E+12	7000.0	0.00	a
103	HCO3 + NO = FACD + NO2 + HO2	5.60E-12	5.60E-12			a
104	HCO3 + HO2 = 0.5 MEPX + 0.5 FACD + 0.2 OH + 0.2 HO2	1.26E-11	5.60E-15	-2300.0	0.00	a
105	ALD2 + O = C2O3 + OH	4.49E-13	1.80E-11	1100.0	0.00	b
106	ALD2 + OH = C2O3	1.50E-11	4.70E-12	-345.0	0.00	a
107	ALD2 + NO3 = C2O3 + HNO3	2.73E-15	1.40E-12	1860.0	0.00	a
108	ALD2 = MEO2 + RO2 + CO + HO2	Photolysis				a
109	ALDX + O = CXO3 + OH	7.02E-13	1.30E-11	870.0	0.00	c,n
110	ALDX + OH = CXO3	1.91E-11	4.90E-12	-405.0	0.00	a
111	ALDX + NO3 = CXO3 + HNO3	6.30E-15	6.30E-15			a
112	ALDX = ALD2 + XO2H + RO2 + CO + HO2	Photolysis				f
113	GLYD + OH = 0.2 GLY + 0.2 HO2 + 0.8 C2O3	8.00E-12	8.00E-12			a
114	GLYD = 0.74 FORM + 0.89 CO + 1.4 HO2 + 0.15 MEOH + 0.19 OH + 0.11 GLY + 0.11 XO2H + 0.11 RO2	Photolysis				a,b,f
115	GLYD + NO3 = HNO3 + C2O3	2.73E-15	1.40E-12	1860.0	0.00	a
116	GLY + OH = 1.8 CO + 0.2 XO2 + 0.2 RO2 + HO2	9.70E-12	3.10E-12	-340.0	0.00	a
117	GLY = 2 HO2 + 2 CO	Photolysis				a,q
118	GLY + NO3 = HNO3 + 1.5 CO + 0.5 XO2 + 0.5 RO2 + HO2	2.73E-15	1.40E-12	1860.0	0.00	a
119	MGLY = C2O3 + HO2 + CO	Photolysis				a
120	MGLY + NO3 = HNO3 + C2O3 + XO2 + RO2	2.73E-15	1.40E-12	1860.0	0.00	a
121	MGLY + OH = C2O3 + CO	1.31E-11	1.90E-12	-575.0	0.00	a
122	H2 + OH = HO2	6.70E-15	7.70E-12	2100.0	0.00	a
123	CO + OH = HO2	2.28E-13	k = k1 + k2[M]			a
		k1	1.44E-13	0.0	0.00	
		k2	3.43E-33	0.0	0.00	
124	CH4 + OH = MEO2 + RO2	6.37E-15	1.85E-12	1690.0	0.00	a
125	ETHA + OH = 0.991 ALD2 + 0.991 XO2H + 0.009 XO2N + RO2	2.41E-13	6.90E-12	1000.0	0.00	a
126	MEOH + OH = FORM + HO2	8.95E-13	2.85E-12	345.0	0.00	a
127	ETOH + OH = 0.95 ALD2 + 0.9 HO2 + 0.1 XO2H + 0.1 RO2 + 0.078 FORM + 0.011 GLYD	3.21E-12	3.00E-12	-20.0	0.00	a
128	KET = 0.5 ALD2 + 0.5 C2O3 + 0.5 XO2H + 0.5 CXO3 + 0.5 MEO2 + RO2 - 2.5 PAR	Photolysis				a
129	ACET = 0.38 CO + 1.38 MEO2 + 1.38 RO2 + 0.62 C2O3	Photolysis				a

Rxn	Reactants = Products	k(298)	A	Ea	B	notes
130	ACET + OH = FORM + C2O3 + XO2 + RO2	1.76E-13	1.41E-12	620.6	0.00	a
131	PRPA + OH = 0.71 ACET + 0.26 ALDX + 0.26 PAR + 0.97 XO2H + 0.03 XO2N + RO2	1.07E-12	7.60E-12	585.0	0.00	a
132	PAR + OH = 0.11 ALDX + 0.76 ROR + 0.13 XO2N + 0.11 XO2H + 0.76 XO2 + RO2 - 0.11 PAR	8.10E-13	8.10E-13			c
133	ROR = 0.2 KET + 0.42 ACET + 0.74 ALD2 + 0.37 ALDX + 0.04 XO2N + 0.94 XO2H + 0.98 RO2 + 0.02 ROR - 2.7 PAR	2.15E+04	5.70E+12	5780.0	0.00	a,c
134	ROR + O2 = KET + HO2	7.67E-15	1.50E-14	200.0	0.00	a,c
135	ROR + NO2 = NTR2	3.29E-11	8.60E-12	-400.0	0.00	a,c
136	ETHY + OH = 0.7 GLY + 0.7 OH + 0.3 FACD + 0.3 CO + 0.3 HO2	7.52E-13	Falloff, F=0.37 ,N=1.30			a
			k₀			
			5.00E-30	0.0	-1.50	
			k∞			
			1.00E-12	0.0	0.00	
137	ETH + O = FORM + HO2 + CO + 0.7 XO2H + 0.7 RO2 + 0.3 OH	7.29E-13	1.04E-11	792.0	0.00	c,o
138	ETH + OH = XO2H + RO2 + 1.56 FORM + 0.22 GLYD	7.84E-12	Falloff, F=0.48 ,N=1.15			a,g
			k₀			
			8.60E-29	0.0	-3.10	
			k∞			
			9.00E-12	0.0	-0.85	
139	ETH + O3 = FORM + 0.51 CO + 0.16 HO2 + 0.16 OH + 0.37 FACD	1.58E-18	9.10E-15	2580.0	0.00	a,g
140	ETH + NO3 = 0.5 NO2 + 0.5 NTR1 + 0.5 XO2H + 0.5 XO2 + RO2 + 1.125 FORM	2.10E-16	3.30E-12	2880.0	0.00	a,g
141	OLE + O = 0.2 ALD2 + 0.3 ALDX + 0.1 HO2 + 0.2 XO2H + 0.2 CO + 0.2 FORM + 0.01 XO2N + 0.21 RO2 + 0.2 PAR + 0.1 OH	3.91E-12	1.00E-11	280.0	0.00	c,o
142	OLE + OH = 0.781 FORM + 0.488 ALD2 + 0.488 ALDX + 0.976 XO2H + 0.195 XO2 + 0.024 XO2N + 1.195 RO2 - 0.73 PAR	2.86E-11	Falloff, F=0.50 ,N=1.13			a,g
			k₀			
			8.00E-27	0.0	-3.50	
			k∞			
			3.00E-11	0.0	-1.00	
143	OLE + O3 = 0.295 ALD2 + 0.555 FORM + 0.27 ALDX + 0.15 XO2H + 0.15 RO2 + 0.334 OH + 0.08 HO2 + 0.378 CO + 0.075 GLY + 0.075 MGLY + 0.09 FACD + 0.13 AACD + 0.04 H2O2 - 0.79 PAR	1.00E-17	5.50E-15	1880.0	0.00	a,g
144	OLE + NO3 = 0.5 NO2 + 0.5 NTR1 + 0.48 XO2 + 0.48 XO2H + 0.04 XO2N + RO2 + 0.5 FORM + 0.25 ALD2 + 0.375 ALDX - PAR	9.54E-15	4.60E-13	1155.0	0.00	a,g
145	IOLE + O = 1.24 ALD2 + 0.66 ALDX + 0.1 XO2H + 0.1 RO2 + 0.1 CO + 0.1 PAR	2.30E-11	2.30E-11			c,o
146	IOLE + OH = 1.3 ALD2 + 0.7 ALDX + XO2H + RO2	5.99E-11	1.05E-11	-519.0	0.00	a,g
147	IOLE + O3 = 0.732 ALD2 + 0.442 ALDX + 0.128 FORM + 0.245 CO + 0.5 OH + 0.3 XO2H + 0.3 RO2 + 0.24 GLY + 0.06 MGLY + 0.29 PAR + 0.08 AACD + 0.08 H2O2	1.57E-16	4.70E-15	1013.0	0.00	a,g
148	IOLE + NO3 = 0.5 NO2 + 0.5 NTR1 + 0.48 XO2 + 0.48 XO2H + 0.04 XO2N + RO2 + 0.5 ALD2 + 0.625 ALDX + PAR	3.70E-13	3.70E-13			a,g
149	ISOP + OH = ISO2 + RO2	9.99E-11	2.70E-11	-390.0	0.00	a
150	ISOP + O = 0.75 ISPD + 0.5 FORM + 0.25 XO2 + 0.25 RO2 + 0.25 HO2 + 0.25 CXO3 + 0.25 PAR	3.00E-11	3.00E-11			0
151	ISO2 + NO = 0.100 INTR + 0.900 NO2 + 0.673 FORM + 0.900 ISPD + 0.818 HO2 + 0.082 XO2H + 0.082 RO2	8.13E-12	2.39E-12	-365.0	0.00	r,s
152	ISO2 + HO2 = 0.88 ISPX + 0.12 OH + 0.12 HO2 + 0.12 FORM + 0.12 ISPD	7.78E-12	7.43E-13	-700.0	0.00	r,s
153	ISO2 + C2O3 = 0.598 FORM + 1.000 ISPD + 0.728 HO2 + 0.072 XO2H + 0.800 MEO2 + 0.200 AACD + 0.872 RO2	1.30E-11	k = kref * K			r,s
		k(ref)	ref = 58			
		K	1.00E+00	0.0	0.00	
154	ISO2 + RO2 = 0.598 FORM + 1.000 ISPD + 0.728 HO2 + 0.072 XO2H + 0.072 RO2	3.48E-13	k = kref * K			r,s
		k(ref)	ref = 70			
		K	1.00E+00	0.0	0.00	

Rxn	Reactants = Products	Rate Parameters				
		k(298)	A	Ea	B	notes
155	ISO2 = HO2 + HPLD	3.30E+09	3.30E+09	8300.0	0.00	j,t
156	ISOP + O3 = 0.6 FORM + 0.65 ISPD + 0.15 ALDX + 0.2 CXO3 + 0.35 PAR + 0.266 OH + 0.2 XO2 + 0.2 RO2 + 0.066 HO2 + 0.066 CO	1.27E-17	1.03E-14	1995.0	0.00	c
157	ISOP + NO3 = 0.35 NO2 + 0.65 NTR2 + 0.64 XO2H + 0.33 XO2 + 0.03 XO2N + RO2 + 0.35 FORM + 0.35 ISPD	6.74E-13	3.03E-12	448.0	0.00	u
158	ISPD + OH = 0.056 XO2N + 0.521 XO2 + 0.238 XO2H + 0.154 MGLY + 0.273 MEO2 + 0.119 GLY + 0.349 GLYD + 0.230 C2O3 + 0.117 CXO3 + 0.236 PAR + 0.256 ACET + 0.197 CO + 0.137 HO2 + 1.088 RO2	3.10E-11	5.58E-12	-511.0	0.00	r,s
159	ISPD + O3 = 0.040 ALD2 + 0.231 FORM + 0.531 MGLY + 0.170 GLY + 0.170 ACET + 0.543 CO + 0.461 OH + 0.150 FACD + 0.398 HO2 + 0.143 C2O3	1.02E-17	3.88E-15	1770.0	0.00	c
160	ISPD + NO3 = 0.717 HNO3 + 0.142 NTR2 + 0.142 NO2 + 0.142 XO2 + 0.142 XO2H + 0.113 GLYD + 0.113 MGLY + 0.717 PAR + 0.717 CXO3 + 0.284 RO2	4.10E-12	4.10E-12	1860.0	0.00	c
161	ISPD = 0.760 HO2 + 0.340 XO2H + 0.160 XO2 + 0.340 MEO2 + 0.208 C2O3 + 0.260 FORM + 0.240 OLE + 0.240 PAR + 0.170 ACET + 0.128 GLYD + 0.840 RO2	Photolysis				c,f
162	ISPX + OH = 0.904 EPOX + 0.933 OH + 0.067 ISO2 + 0.067 RO2 + 0.029 IOLE + 0.029 ALDX	7.77E-11	2.23E-11	-372.0	0.00	r,s
163	HPLD = OH + HO2 + ISPD	Photolysis				r,s
164	HPLD + NO3 = HNO3 + ISPD	1.17E-14	6.00E-12	1860.0	0.00	r,s
165	EPOX + OH = EPX2 + RO2	1.51E-11	5.78E-11	400.0	0.00	r,s
166	EPX2 + HO2 = 0.275 GLYD + 0.275 GLY + 0.275 MGLY + 1.125 OH + 0.825 HO2 + 0.375 FORM + 0.074 FACD + 0.251 CO + 2.175 PAR	7.78E-12	7.43E-13	-700.0	0.00	r,s
167	EPX2 + NO = 0.275 GLYD + 0.275 GLY + 0.275 MGLY + 0.125 OH + 0.825 HO2 + 0.375 FORM + NO2 + 0.251 CO + 2.175 PAR	8.13E-12	2.39E-12	-365.0	0.00	r,s
168	EPX2 + C2O3 = 0.22 GLYD + 0.22 GLY + 0.22 MGLY + 0.1 OH + 0.66 HO2 + 0.3 FORM + 0.2 CO + 1.74 PAR + 0.8 MEO2 + 0.2 AACD + 0.8 RO2	1.30E-11 k(ref) K	k = kref * K ref = 58 1.00E+00	0.0	0.00	a,r,s
169	EPX2 + RO2 = 0.275 GLYD + 0.275 GLY + 0.275 MGLY + 0.125 OH + 0.825 HO2 + 0.375 FORM + 0.251 CO + 2.175 PAR + RO2	3.48E-13 k(ref) K	k = kref * K ref = 70 1.00E+00	0.0	0.00	a,r,s
170	INTR + OH = 0.63 XO2 + 0.37 XO2H + RO2 + 0.444 NO2 + 0.185 NO3 + 0.104 INTR + 0.592 FORM + 0.331 GLYD + 0.185 FACD + 2.7 PAR + 0.098 OLE + 0.078 ALDX + 0.266 NTR2	3.10E-11	3.10E-11			r,s
171	TERP + O = 0.15 ALDX + 5.12 PAR	3.60E-11	3.60E-11			c
172	TERP + OH = 0.75 XO2H + 0.5 XO2 + 0.25 XO2N + 1.5 RO2 + 0.28 FORM + 1.66 PAR + 0.47 ALDX	6.77E-11	1.50E-11	-449.0	0.00	c
173	TERP + O3 = 0.57 OH + 0.07 XO2H + 0.69 XO2 + 0.18 XO2N + 0.94 RO2 + 0.24 FORM + 0.001 CO + 7 PAR + 0.21 ALDX + 0.39 CXO3	7.63E-17	1.20E-15	821.0	0.00	c
174	TERP + NO3 = 0.47 NO2 + 0.28 XO2H + 0.75 XO2 + 0.25 XO2N + 1.28 RO2 + 0.47 ALDX + 0.53 NTR2	6.66E-12	3.70E-12	-175.0	0.00	c
175	BENZ + OH = 0.53 CRES + 0.352 BZO2 + 0.352 RO2 + 0.118 OPEN + 0.118 OH + 0.53 HO2	1.22E-12	2.30E-12	190.0	0.00	a,d,e
176	BZO2 + NO = 0.918 NO2 + 0.082 NTR2 + 0.918 GLY + 0.918 OPEN + 0.918 HO2	9.04E-12	2.70E-12	-360.0	0.00	d,h
177	BZO2 + C2O3 = GLY + OPEN + HO2 + MEO2 + RO2	1.30E-11 k(ref)	k = kref * K ref = 58			a,d,h

Rxn	Reactants = Products	Rate Parameters				
		k(298)	A	Ea	B	notes
		K	1.00E+00	0.0	0.00	
178	BZO2 + HO2 =	1.49E-11	1.90E-13	-1300.0	0.00	d
179	BZO2 + RO2 = GLY + OPEN + HO2 + RO2	3.48E-13	k = kref * K			a,d,h
		k(ref)	ref = 70			
		K	1.00E+00	0.0	0.00	
180	TOL + OH = 0.18 CRES + 0.65 TO2 + 0.72 RO2 + 0.1 OPEN + 0.1 OH + 0.07 XO2H + 0.18 HO2	5.63E-12	1.80E-12	-340.0	0.00	a,d,e
181	TO2 + NO = 0.86 NO2 + 0.14 NTR2 + 0.417 GLY + 0.443 MGLY + 0.66 OPEN + 0.2 XOPN + 0.86 HO2	9.04E-12	2.70E-12	-360.0	0.00	d,h
182	TO2 + C2O3 = 0.48 GLY + 0.52 MGLY + 0.77 OPEN + 0.23 XOPN + HO2 + MEO2 + RO2	1.30E-11	k = kref * K			a,d,h
		k(ref)	ref = 58			
		K	1.00E+00	0.0	0.00	
183	TO2 + HO2 =	1.49E-11	1.90E-13	-1300.0	0.00	d
184	TO2 + RO2 = 0.48 GLY + 0.52 MGLY + 0.77 OPEN + 0.23 XOPN + HO2 + RO2	3.48E-13	k = kref * K			a,d,h
		k(ref)	ref = 70			
		K	1.00E+00	0.0	0.00	
185	XYL + OH = 0.155 CRES + 0.544 XLO2 + 0.602 RO2 + 0.244 XOPN + 0.244 OH + 0.058 XO2H + 0.155 HO2	1.85E-11	1.85E-11			d,e,p
186	XLO2 + NO = 0.86 NO2 + 0.14 NTR2 + 0.221 GLY + 0.675 MGLY + 0.3 OPEN + 0.56 XOPN + 0.86 HO2	9.04E-12	2.70E-12	-360.0	0.00	d,h
187	XLO2 + HO2 =	1.49E-11	1.90E-13	-1300.0	0.00	d
188	XLO2 + C2O3 = 0.26 GLY + 0.77 MGLY + 0.35 OPEN + 0.65 XOPN + HO2 + MEO2 + RO2	1.30E-11	k = kref * K			a,d,h
		k(ref)	ref = 58			
		K	1.00E+00	0.0	0.00	
189	XLO2 + RO2 = 0.26 GLY + 0.77 MGLY + 0.35 OPEN + 0.65 XOPN + HO2 + RO2	3.48E-13	k = kref * K			a,d,h
		k(ref)	ref = 70			
		K	1.00E+00	0.0	0.00	
190	CRES + OH = 0.025 GLY + 0.025 OPEN + HO2 + 0.2 CRO + 0.732 CAT1 + 0.02 XO2N + 0.02 RO2	4.12E-11	1.70E-12	-950.0	0.00	d
191	CRES + NO3 = 0.3 CRO + HNO3 + 0.48 XO2 + 0.12 XO2H + 0.24 GLY + 0.24 MGLY + 0.48 OPO3 + 0.1 XO2N + 0.7 RO2	1.40E-11	1.40E-11			d
192	CRO + NO2 = CRON	2.10E-12	2.10E-12			d
193	CRO + HO2 = CRES	5.50E-12	5.50E-12			d
194	CRON + OH = NTR2 + 0.5 CRO	1.53E-12	1.53E-12			d
195	CRON + NO3 = NTR2 + 0.5 CRO + HNO3	3.80E-12	3.80E-12			a,d
196	CRON = HONO + HO2 + FORM + OPEN	Photolysis				d
197	XOPN = 0.4 GLY + XO2H + 0.7 HO2 + 0.7 CO + 0.3 C2O3	Photolysis				d,p
198	XOPN + OH = MGLY + 0.4 GLY + 2.0 XO2H + 2.0 RO2	9.00E-11	9.00E-11			d,p
199	XOPN + O3 = 1.2 MGLY + 0.5 OH + 0.6 C2O3 + 0.1 ALD2 + 0.5 CO + 0.3 XO2H + 0.3 RO2	2.02E-17	1.08E-16	500.0	0.00	d,p
200	XOPN + NO3 = 0.5 NO2 + 0.5 NTR2 + 0.45 XO2H + 0.45 XO2 + 0.1 XO2N + RO2 + 0.25 OPEN + 0.25 MGLY	3.00E-12	3.00E-12			d,p
201	OPEN = OPO3 + HO2 + CO	Photolysis				d,p
202	OPEN + OH = 0.6 OPO3 + 0.4 XO2H + 0.4 RO2 + 0.4 GLY	4.40E-11	4.40E-11			d,p
203	OPEN + O3 = 1.4 GLY + 0.24 MGLY + 0.5 OH + 0.12 C2O3 + 0.08 FORM + 0.02 ALD2 + 1.98 CO + 0.56 HO2	1.01E-17	5.40E-17	500.0	0.00	d,p
204	OPEN + NO3 = OPO3 + HNO3	3.80E-12	3.80E-12			d,p
205	CAT1 + OH = 0.14 FORM + 0.2 HO2 + 0.5 CRO	5.00E-11	5.00E-11			d
206	CAT1 + NO3 = CRO + HNO3	1.70E-10	1.70E-10			d
207	OPO3 + NO = NO2 + 0.5 GLY + 0.5 CO + 0.8 HO2 + 0.2 CXO3	1.00E-11	1.00E-11			d

Rxn	Reactants = Products	Rate Parameters				
		k(298)	A	Ea	B	notes
208	OPO3 + NO2 = OPAN	9.40E-12	k = kref * K			a, l
		k(ref)	ref = 54			
		K	1.00E+00	0.0	0.00	
209	OPAN = OPO3 + NO2	2.98E-04	k = kref * K			a, l
		k(ref)	ref = 55			
		K	1.00E+00	0.0	0.00	
210	OPO3 + HO2 = 0.41 PACD + 0.15 AACD + 0.15 O3 + 0.44 ALDX + 0.44 XO2H + 0.44 RO2 + 0.44 OH	1.39E-11	k = kref * K			d
		k(ref)	ref = 57			
		K	1.00E+00	0.0	0.00	
211	OPO3 + C2O3 = MEO2 + XO2 + ALDX + 2 RO2	1.55E-11	k = kref * K			d
		k(ref)	ref = 59			
		K	1.00E+00	0.0	0.00	
212	OPO3 + RO2 = 0.8 XO2H + 0.8 ALDX + 1.8 RO2 + 0.2 AACD	1.30E-11	k = kref * K			d
		k(ref)	ref = 58			
		K	1.00E+00	0.0	0.00	
213	OPAN + OH = 0.5 NO2 + 0.5 GLY + CO + 0.5 NTR2	3.60E-11	3.60E-11			w
214	PANX + OH = NO2 + ALD2	3.00E-12	2.00E-12			
215	NTR2 = HNO3	4.60E-05	4.60E-05			x

Notes:

a   IUPAC (2010): IUPAC Subcommittee for Gas Kinetic Data Evaluation web site, http://www.iupac-kinetic.ch.cam.ac.uk/

b   NASA/JPL (2006): Sander, S.P., R.R. Friedl, D. M. Golden, M. J. Kurylo, G. K. Moortgat, P. H. Wine, A. R. Ravishankara, C. E. Kolb, M. J. Molina, B. J Finlayson-Pitts, R. E. Huie and V. L. Orkin (2006). "Chemical Kinetics and Photochemical Data for use in Atmospheric Studies, Evaluation Number 15. NASA Jet Propulsion Laboratory." July 2006, Available from: http://jpldataeval.jpl.nasa.gov/download.html.

c   Yarwood, G., Rao, S., Yocke, M., Whitten, G.Z., 2005. Updates to the Carbon Bond mechanism: CB05. Report to the U.S. Environmental Protection Agency, December 2005. (http://www.camx.com/publ/pdfs/CB05_Final_Report_120805.pdf)

d   Whitten, G.Z., Heo, G., Kimura, Y., McDonald-Buller, E., Allen, D.T., Yarwood, G. (2010). A new condensed toluene mechanism for Carbon Bond: CB05-TU, Atmospheric Environment (2010), doi: 10.1016/j.atmosenv.2009.12.029. (http://dx.doi.org/10.1016/j.atmosenv.2009.12.029; in press)

e   Bloss, C., Wagner, V., Jenkin, M.E., Volkamer, R., Bloss, W.J., Lee, J.D., Heard, D.E., Wirtz, K., Martin-Reviejo, M., Rea, G., Wenger, J.C., Pilling, M.J., 2005. Development of a detailed chemical mechanism (MCMv3.1) for the atmospheric oxidation of aromatic hydrocarbons. Atmospheric Chemistry and Physics 5, 641-644.

f   Carter, W.P.L., 2000. Documentation of the SAPRC-99 chemical mechanism for VOC reactivity assessment, Report to the California Air Resources Board, Contracts 92-329 and 95-308. (http://www.cert.ucr.edu/~carter/absts.htm#saprc99)

g   Calvert, J.G., R. Atkinson, J.A. Kerr, S. Madronich, G.K. Moortgat, T.J. Wallington, G. Yarwood. 2000. The mechanisms of atmospheric oxidation of the alkenes. Oxford University Press

h   Arey, J., Obermeyer, G., Aschmann, S.M., Chattopadhyay, S., Cusick, R.D., Atkinson, R., 2009. Dicarbonyl products of the OH radical-initiated reaction of a series of aromatic hydrocarbons. Environmental Science & Technology 43, 683-689.

i   Hu, D., Tolocka, M., Li, Q., Kamens, R.M., 2007. A kinetic mechanism for predicting secondary organic aerosol formation from toluene oxidation in the presence of NOx and natural sunlight. Atmospheric Environment 41, 6478–6496.

j   Archibald, A.T., Cooke, M.C., Utembe, S.R., Shallcross, D.E., Derwent, R.G., Jenkin, M.E., 2010. Impacts of mechanistic changes on HOx formation and recycling in the oxidation of isoprene. Atmospheric Chemistry and Physics Discussion 10, 5863-5910. (www.atmos-chem-phys-discuss.net/10/5863/2010).

k   Hjorth, J., J. Notholt, and G. Restelli 1992 "A spectroscopic study of the equilibrium NO2 + NO3 + M = N2O5 + M and the kinetics of the O3/N2O5/NO3/NO2/air system" Int. J. Chem. Kinet., 24, 51-65.

l   The IUPAC (a) data sheets for PAN formation/destruction erroneously list n=1.0 rather than n=1.44

m   Jeffries, H.E., I. Voicu, and K. Sexton. 2002. "Experimental Tests of Reactivity and Re-evaluation of The Carbon Bond Four Photochemical Reaction Mechanism." Final report for Cooperative Agreement No. R828906, U.S. EPA, RTP, NC.

n   Herron, J.T. 1988 "Evaluated chemical kinetic data for the reactions of atomic oxygen O(3P) with saturated organic compounds in the gas phase" J. Phys. Chem. Ref. Data, 17, 967.

o   Cvetanovic, R.J. 1987. "Evaluated chemical kinetic data for the reactions of atomic oxygen O(3P) with unsaturated hydrocarbons." J. Phys. Chem. Ref. Data, 16, 261.

p   Calvert, J. G., Atkinson, R., Becker, K.H., Kamens, R.M., Seinfeld, J.H., Wallington, T.J., Yarwood, G., 2002. The Mechanisms of Atmospheric Oxidation of Aromatic Hydrocarbons, Oxford University Press, New York, 566p.

q   Feierabend, K.J., Flad, J.E., Brown, S.S., Burkhold, J.B., 2009. HCO quantum yields in the photolysis of HC(O)C(O)H (glyoxal) between 290 and 420 nm. J. Phys. Chem. A 113, 7784-7794.

r   Paulot, F., Crounse, J.D., Kjaergaard, H.G., Kroll, J.H., Seinfeld, J.H., Wennberg, P.O., 2009a. Isoprene photooxidation: new insights into the production of acids and organic nitrates. Atmospheric Chemistry and Physics 9, 1479-1501.

s   Paulot, F., Crounse, J.D., Kjaergaard, H.G., Kürten, A., St. Clair, J.M., Seinfeld, J.H., Wennberg, P.O., 2009b. Unexpected expoxide formation in the gas-phase photooxidation of isoprene. Science 325, 730-733.

t   Peeters, J., Nguyen, T.L., Vereecken, L., 2009. HOx radical regeneration in the oxidation of isoprene. Physical Chemistry and Chemical Physics 11, 5935-5939.

u   Perring, A.E., A. Wisthaler, M. Graus, P.J. Wooldridge, A.L. Lockwood, L.H. Mielke, P.B. Shepson, A. Hanset, and R.C. Cohen (2009) "A product study of the isoprene+NO_3 reaction." Atmospheric Chemistry and Physics, 9, 4945-4956

v   Mollner, A.K., S. Valluvadasan, L. Feng, M. K. Sprague, M. Okumura, D. B. Milligan, W. J. Bloss, S. P. Sander, P. T. Martien, R. A. Harley, A. B. McCoy, W. P. L. Carter (2010) "Rate of Gas Phase Association of Hydroxyl Radical and Nitrogen Dioxide.", Science 330, 646 DOI: 10.1126/science.1193030

w   http://mcm.leeds.ac.uk/MCM/home.htt

x   Liu, S., Shilling, J. E., Song, C., Hiranuma, N., Zaveri, R. A., & Russell, L. M. (2012). Hydrolysis of organonitrate functional groups in aerosol particles. Aerosol Science and Technology, 46(12), 1359-1369.